

**PARAMETRIC REPRESENTATION OF THE PRIMARY HURRICANE VORTEX.
PART II:
A NEW FAMILY OF SECTIONALLY CONTINUOUS PROFILES**

H. E. Willoughby¹

*International Hurricane Research Center, Florida International University, Miami,
Florida*

R. W. R. Darling

National Security Agency, Annapolis Junction, Maryland

M. E. Rahn²

Hurricane Research Division/AOML/NOAA, Miami, Florida

4 January 2005

¹ *Corresponding author address:* H. E. Willoughby, International Hurricane Research Center, 360 MARC Building, University Park Campus, Florida International University, Miami FL 33199
E-mail: hugh.willoughby@fiu.edu

² Deceased

Abstract

For applications such as windstorm underwriting or storm-surge forecasting, hurricane wind profiles are often approximated by continuous functions that are zero at the vortex center, increase to a maximum in the eyewall, and then decrease asymptotically to zero far from the center. Comparisons between the most commonly used functions and aircraft observations reveal systematic errors. Although winds near the peak are too strong, they decrease too rapidly with distance away from the peak. Pressure-wind relations for these profiles typically overestimate maximum winds.

A promising alternative is a family of sectionally continuous profiles in which the wind increases as a power of radius inside the eye and decays exponentially outside the eye after a smooth polynomial transition across the eyewall. Based upon a sample of 493 observed profiles, the mean exponent for the power law is 0.79 and the mean decay length is 243 km. The database actually contains 606 aircraft sorties, but 113 of these failed quality-control screening. Hurricanes stronger than Saffir-Simpson category 2 often require two exponentials to match the observed rapid decrease of wind with radius just outside the eye and slower decrease farther away. Experimentation showed that a fixed value of 25 km was satisfactory for the faster decay length. The mean value of the slower was 295 km. The mean contribution of the faster exponential to the outer profile was 0.10, but for the most intense hurricanes it sometimes exceeded 0.5. The power-law exponent and proportion of the faster decay length increased with maximum wind speed and decreased with latitude; whereas the slower decay length decreased with intensity and increased with latitude, consistent with the qualitative observation that more intense hurricanes in lower latitudes usually have more sharply peaked wind profiles.

1. Introduction

In the first paper of this series (Willoughby and Rahn 2004, hereafter Part I), we showed that the most commonly used analytical representation of hurricane winds' radial structure (Holland 1980) suffers from systematic errors. Comparisons between statistically fitted profiles and nearly 500 tropical cyclones observed by aircraft demonstrated that, although the analytical profiles overestimate the width of the eyewall wind maximum, the wind decreases too rapidly with distance from the maximum both inside and outside the eye. Since variants of Holland's profile are fundamental to applications such as modeling of storm surge (Jelesnianski 1967) or windstorm risk (e.g. Vickery and Twisdale, 1995), these shortcomings highlight the need for a more realistic alternative.

Tropical cyclones are nearly circular vortices with damaging winds concentrated in and around the eyewall. The geometric center of the clear eye or the stagnation point inside the eye defines a vortex center that can be tracked objectively. Thus, the center position and intensity, measured in terms of maximum wind or minimum sea-level pressure, provide a first-order characterization of tropical cyclones. Indeed, the HURDAT file (Jarvinen et al. 1984), which constitutes the authoritative long-term hurricane climatology, contains exactly that information. The role of "parametric" profiles is to convert position and intensity into a geographical distribution of winds. The Holland profile employs three parameters, maximum wind, radius of maximum wind, and B an exponent that sets the sharpness of the eyewall wind maximum. A key result of Part I was that, even for an optimally chosen B , the second derivative of the wind with respect to radius is too small near the radius of maximum where the profile is concave downward and too large away from the maximum where the profile is concave upward. Here we

propose a new family of parametric profiles that do not suffer from these limitations. The profile wind is proportional to a power of radius inside the eye and decays exponentially outside the eye with a smooth transition across the eyewall. Least squares fits of these profiles to the same sample of aircraft observations used in Part I validates them and provides statistical estimates of their parameters. Section 2 of this paper formulates the new family of profiles and describes the least-squares fitting procedure. Subsequent sections present profiles with a single outer exponential decay length, and with a superposition of two outer exponentials. Section 5 considers alternative profile formulations and addresses hydrodynamic stability of the fitted vortices. Section 6 summarizes results and draws conclusions.

2. Analysis

a. Profile formulation

Piecewise continuous wind profiles (e.g. Willoughby 1995) show promise as an alternative to the Holland model. They are composed of analytical segments patched smoothly together (Fig. 1). Inside the eye the wind increases in proportion to a power of radius. Outside the eye, the wind decays exponentially with a radial e-folding distance that changes from storm to storm. The transition across the radius of maximum wind from the inner to outer profiles is accomplished with a smooth, radially varying polynomial ramp function.

$$V(r) = V_i = V_{\max} \left(\frac{r}{R_{\max}} \right)^n, \quad (0 \leq r \leq R_1), \quad (1.1)$$

$$V(r) = V_i(1 - w) + V_o w, \quad (R_1 \leq r \leq R_2), \quad (1.2)$$

$$V(r) = V_o = V_{\max} \exp \left\{ -\frac{r - R_{\max}}{X_1} \right\}, \quad (R_2 \leq r), \quad (1.3)$$

Here V_i , V_e , and V_o are the tangential wind component in the eye, in the eyewall transition, and beyond the transition zone, which lies between $r = R_1$ and $r = R_2$. V_{\max} and R_{\max} are the maximum wind and radius at which the maximum wind occurs. X_1 is the exponential decay length in the outer vortex and n is the exponent for the power law inside the eye. Note that both V_i and V_o are defined throughout the transition zone and that both are equal to V_{\max} at $r = R_{\max}$.

The weighting function, w , is expressed in terms of a nondimensional argument $\xi = (r - R_1)/(R_2 - R_1)$. When $\xi \leq 0$, $w = 0$; when $\xi \geq 1$, $w = 1$. In the subdomain $0 \leq \xi \leq 1$, the weighting is defined as the polynomial:

$$w(\xi) = 126\xi^5 - 420\xi^6 + 540\xi^7 - 315\xi^8 + 70\xi^9, \quad (2)$$

which ramps up smoothly from zero to one between R_1 and R_2 . As described in the Appendix, the weighting function is derived by integration of a bell-shaped polynomial curve given by $C[\xi(1 - \xi)]^k$ when $(0 \leq \xi \leq 1)$ and zero elsewhere. The coefficient C is chosen to make $w(1) = 1$, and the exponent k is the “order” of the bell and ramp curves, even though the resulting polynomials are of order $2k$ and $2k + 1$, respectively. We have coined the term “bellramp” functions to denote this family of polynomials.

Based upon parameters R_{\max} , V_{\max} , X_1 , and n , the full wind profile is constructed as follows. First, the width of the transition $R_1 - R_2$ is specified *a-priori* at a value between 10 and 25 km. Then, the location of the transition zone is determined by requiring the radial derivative of (1.2) to vanish at $r = R_{\max}$, recognizing that $V_i(R_{\max}) = V_o(R_{\max}) = V_{\max}$. This condition yields the value of w at the wind maximum:

$$w\left(\frac{R_{\max} - R_1}{R_2 - R_1}\right) = -\frac{\frac{\partial V_i}{\partial r}}{\frac{\partial V_o}{\partial r} + \frac{\partial V_i}{\partial r}} = \frac{nX_1}{R_{\max} + nX_1}, \quad (3)$$

which may be solved for R_1 through numerical inversion of (2).

As shown subsequently, in many situations the profile described by (1.1-1.3) suffers from the problem that vexed the Holland profile in Part I. Relatively large values of X_1 chosen to generate profiles that match the outer part of the vortex may fail to capture the rapid decrease of wind just outside the eyewall; conversely smaller values of X_1 generate profiles that match the steep gradient outside the eyewall decrease too rapidly farther from the center. Often there is no intermediate value that can fit the observations in both parts of the domain. Although this difficulty is a less pronounced than for the Holland profile, it is still problematic. A remedy entails replacement of the single exponential with the sum two exponentials with e-folding lengths X_1 and X_2 .

$$V_o = V_{\max} \left[(1 - A) \exp\left\{-\frac{r - R_{\max}}{X_1}\right\} + A \exp\left\{-\frac{r - R_{\max}}{X_2}\right\} \right], \quad (R_2 \leq r), \quad (4)$$

where the parameter A sets the relative contribution of the two exponentials to the profile. Figure 2 illustrates application of (4) to Hurricane Diana of 1984. Clearly, the dual-exponential profile captures the profile's sharpness at the radius of maximum wind as well as the more gradual decrease of wind at radii farther from the eyewall.

There is an issue of non-uniqueness in this formulation. Several different combinations of X_1 , X_2 and A can often fit a given set of observations equally well. This situation complicates statistical estimation of the profile parameters, so that we generally fit A and one variable decay length, keeping the other decay length, usually the shorter

one, fixed. Thus, most of this paper will deal with either single-exponential profiles or dual-exponential profiles with one predetermined decay length.

In this formulation, unlike the Holland profile, there is no closed-form relation for the gradient-balance geopotential height in terms of the vortex parameters. Thus, the geopotential height is computed through outward numerical integration of the gradient wind acceleration from the observed height at the vortex center of the standard isobaric surface nearest flight level.

$$Z(r) = Z_c + \frac{1}{g} \int_0^r \left(\frac{V^2(r')}{r'} + fV(r') \right) dr' , \quad (5)$$

where $Z(r)$ is the height of the specified surface, Z_c is $Z(0)$, and g is the acceleration of gravity. Setting the upper bound on the integral to infinity in (5) produces a gradient balance estimate of the undisturbed geopotential around the storm, $Z_e = Z(r \rightarrow \infty)$.

Based this integral it is possible to relate V_{\max} to $Z_e - Z_c$ in order to devise height-wind relations for the single exponential and dual exponential profiles. A key advantage of using exponential functions to describe the outer profile is that it guarantees a well-behaved height-wind relationship as well as finite values for vortex total relative angular momentum and kinetic energy.

b. Profile fitting.

Single-exponential profiles have four parameters R_{\max} , V_{\max} , X_I , and n . Dual-exponential profiles with one predetermined decay length have five parameters (R_{\max} , V_{\max} , X_I , A , and n), and dual-exponential profiles with both decay lengths free have six parameters (R_{\max} , V_{\max} , X_I , X_2 , A , and n). As in Part I, V_{\max} and R_{\max} are determined by scanning each profile for the strongest reported wind and its radial position. This

procedure leaves the single-exponential, constrained dual-exponential, and free dual-exponential profiles, respectively, with two, three and four parameters that require least-squares fitting to the data. The cost function is the same as that used in Part I,

$$S^2 = \sum_{k=1}^K \left(v_o(r_k) - v_g(r_k, n, X_1, \dots) \right)^2 + g(z_o(r_k) - z(r_k, n, X_1, \dots))^2 L_z^{-1}. \quad (6)$$

It is the summed squares of the differences between the profile and observed tangential wind and between the computed geopotential height (5) and the observed height of the isobaric surface nearest the aircraft flight level. Since the parameter space has relatively few dimensions and the cost function is essentially a parabola, we use the simplex algorithm (Nelder and Meade 1965, Press et al. 1986) to find the minimum value of S^2 . L_z is a Lagrange multiplier that sets the strength of the gradient balance constraint and also makes (6) dimensionally homogeneous with units of velocity squared. Here we set $L_z = 1 \text{ km}$, the same value used in Part I.

Ranges of the fitted parameters are constrained with Lagrange multipliers, for example, $0.4 \leq n \leq 2.4$ or $0 \leq A \leq 1$, to prevent the algorithm from wandering into physically unrealistic parts of the parameter space. Typical minimum values of S^2 are a few hundred to a few thousand $\text{m}^2 \text{s}^{-2}$, and the penalties imposed outside the preferred subdomain by the Lagrangian constraints are $2\text{--}5 \times 10^3 \text{ m}^2 \text{s}^{-2}$. The constraints generally have limited effect on the fitted parameters inasmuch as the simplex algorithm almost always finds values within the preferred subdomain. Two exceptions to this generality are $A = 0$ or 1 , which characterize profiles where X_1 or X_2 can represent the shape of the “dual exponential” outer profile completely. The constraint on the minimum decay lengths generally is set for values greater than 50-100 km, but the minimization algorithm seldom selects values that small. By contrast, the upper bound on decay lengths does

exert significant control over the fitted profiles. In some tropical cyclones where the wind remains fairly constant from just outside the eyewall to the sampling domain boundary, the unconstrained algorithm will seek decay lengths ≥ 1000 km. Since the values of Z_e that result from integration of (5) in these situations can be greater than, Z_a , from climatologically representative soundings (Jordan 1958, Sheets 1969), we generally set an upper bound of a few hundred kilometers on the longer decay length. Tuning of this constraint is discussed extensively in the next two sections, inasmuch as it is important to obtaining realistic fits.

The data for the least-squares fits are the same as those used in Part I. They contain 606 logical sorties into Atlantic and Eastern Pacific tropical storms and hurricanes flown by NOAA and Air Force Reserve aircraft between 1977 and 2000 and are representative in terms of its geographical and seasonal distribution. They are divided into “logical sorties,” each a series of successive transects across the tropical-cyclone center at fixed altitude, usually flown by one aircraft during the course of a few hours. Although there are a few sorties with 300 km domains, most extend to ≤ 150 km. The variables are expressed in a cylindrical coordinate system that moves along the objectively determined cyclone track. The observed dynamic and kinematic variables are transformed into vortex-centered coordinates and averaged azimuthally around the vortex to produce a profile composite (PCMP) file for each sortie. The least squares fits use the PCMP files. Predominant flight levels were 850 and 700 hPa (1.5 and 3 km), but some missions (generally in weaker storms) were flown as low as 950 hPa (500 m) and as high as 400 hPa (7 km). Although depressions and weak tropical storms are underrepresented, the sample is reasonably representative in terms of cyclone intensity. Of the original

sample, 113 failed quality control (QC) criteria that screened out profiles where the radius of maximum was more than half the sampling domain or where the data fail to describe a well-defined dynamic center inside the eye. The 493 PCMP files that met the QC criteria are homogeneous with the sample used in Part I.

2. Single-exponential profile

The single-exponential profile is the simplest of the new functional forms. Since the Lagrange-multiplier constraint on the maximum value of X_1 is the only tuning required, we examine its effect first, by a series of five least-squares fits to the entire sample with $X_1 \leq 200, 400, 600, 800$ and 1000 km (Fig 3a). The mean value of X_1 increases from 203 to 249 km over this range of upper bounds. For most individual sorties, the constraint has no effect, but for a few the fitting algorithm selects larger values of X_1 , increasing the sample average, as the constrained upper bound increases. If one compares the average difference between Z_e , the computed environmental geopotential height from (5) and Z_a , the climatologically expected value, the computed values are always too low, despite the problem with too-large values of X_1 for some sorties. The value of $Z_e - Z_a$ increases from -18.3 m when the constraint requires $X_1 \leq 200$ km to -5.4 m when $X_1 \leq 1000$ (Fig. 3b). Most of the increase happens between $X_1 \leq 200$ km and $X_1 \leq 600$ km. It is important to recognize that the decrease in magnitude of the negative environmental-height bias stems from compensating errors. For most PCMP files, the single-exponential fitting algorithm selects too-small values of X_1 that lead to underestimated values of Z_e . Relaxing the upper constraint on X_1 causes a few PCMP files to produce overestimates of Z_e , which increases the average toward the hoped-for zero bias. For this reason, we set the decay length Lagrange multiplier

constraint to $50 \leq X_1 \leq 600$ km which produces $Z_e - Z_a = -7.4$ m. This value of the constraint produces mean parameters, $n = 0.79 \pm 0.34$ and $X_1 = 243 \pm 141$ km. The mean difference between the fitted and observed winds is essentially zero, and the rms error is 2.5 m s^{-1} (dependant data). The bias and rms errors in geopotential height are 1.3 and 10.4 m. The positive Z bias is confined inside the 150 km domain where the curve fitting is done. The bias reverses as integral in (5) is continued beyond 150 km, where V decreases too rapidly with distance from the vortex center.

For Hurricane Anita of 1977 (Fig. 4), chronologically the first tropical cyclone in the data base, the fitting algorithm selects $n = 1.16$ and $X_1 = 100.7$ km as the optimum fit. The rms wind and height errors are larger than average for single-exponential profiles, 4.6 m s^{-1} and 18.8 m, respectively, with essentially zero wind bias and 5.4 m positive height bias. Comparison of the wind and geopotential height variations shows a negative height bias due to underestimation of the wind inside the eye. The bias changes over to positive beyond about twice the eye radius because the fitted winds are too strong outside the eye. Farther from the center, the negative height bias decreases in magnitude slowly because the fitted winds are too weak beyond 100 km radius. It is disappointing to see this pattern of errors emerge here because it is similar, though less pronounced, to the one that characterized the Holland profile in Part I.

The single-exponential profile depicts other tropical cyclones with somewhat more fidelity. In Part I, Hurricane Mitch of 1998 was one of the most successful Holland-profile fits. Here, the single-exponential fit (Fig 5a, $n = 0.69$, $X_1 = 119$ km) does about as well, although the wind maximum is too actually narrow. The Holland fit to Hurricane Hugo of 1989 was a less successful because the fitted wind maximum was too broad and

the wind decreased too rapidly with radius beyond 80 km radius. The corresponding single-exponential profile (Fig 5b, $n = 1.67$, $X_1 = 145$ km) fitted both the primary wind maximum and the profile within 120 km of the center closely, but could not represent the outer wind maximum present beyond 120 km radius. Despite improvements with the sectionally continuous fitted profiles, both Mitch and Hugo exhibit the same error that appeared in Anita and in the Holland profiles.

Edouard of 1996 was another successful Holland profile because its broad wind maximum and gradual decrease of wind outside the eye could be fitted by the Holland profile with a relatively small value of $B = 0.86$. The single-exponential fit (Fig 5c, $n = 0.41$, $X_1 = 588$ km), with its small exponent inside the eye and long decay length, captures most features of the data except for the broad shoulder of the profile inward from the wind maximum. Erika of 1997 was a relatively unsuccessful Holland fit because the Holland profile was unable to match its sharp wind maximum, even with a relatively large $B = 1.17$. The single-exponential profile (Fig. 5d, $n = 0.581$, $X_1 = 178$ km) was able to represent its shape more accurately. Thus, despite some limitations, the added degrees of freedom here produce significant improvement over the Holland formulation.

Description of hurricane wind profiles in terms the sample-mean values of n and X_1 misses systematic variations of vortex structure because all four parameters of the single-exponential profile are correlated with each other. A regression line fitted to X_1 decreases from 368 km to 86 km as V_{\max} increases from 10 to 70 m s⁻¹ (Fig 6a). Over the same interval, n increases from 0.43 to 1.24 (Fig 6b). Although the slopes of both curves differ from zero at better than 1% significance, there is considerable scatter around the regression lines. In Fig. 6a, the points that cluster near $X_1 = 600$ km and V_{\max} between 10

and 42 m s^{-1} have values limited by the Lagrange multiplier constraint; whereas the others are unaffected. Only a few of the n values in Fig. 6b approach the Lagrange multiplier limits.

The means, standard deviations, and the correlation matrix among the parameters (Table 1a) summarize all possible linear relations. As shown in Part I, these statistics contain enough information to prepare linear estimators of the parameters. The eigenvalues and eigenvectors of the correlation matrix (Table 1b) reveal systematic patterns of variation. The leading eigenvector, $E1$, which explains $>50\%$ of the parameter standardized variance, delineates increasing n and decreasing X_1 correlated with increasing V_{\max} , decreasing latitude, and decreasing $\ln R_{\max}$. In qualitative terms, $E1$ depicts shrinking of the eye and sharpening of the eyewall wind maximum with increasing intensity and lower latitude. It is the same physical association as the “convective ring” leading eigenvector in Part I where decreasing R_{\max} and increasing B were associated with intensification and lower latitude. In both cases, sharpening of the eyewall wind maximum and shrinking of the eye in more intense hurricanes is consistent with the response of balanced hurricane-like vortices to heating around the eye (Smith 1981, Shapiro and Willoughby 1982, and Schubert and Hack 1982). The second eigenvector, $E2$, projects almost entirely onto latitude, associated to some extent with intensity. The qualitative impression is that tropical cyclones in the early and late stages of their life cycles, where intensification through convective heating is either not well established or has run its course, project onto $E2$. $E1$ and $E2$ combined explain $> 70\%$ of the standardized parameter variance. It is difficult to advance physical interpretations for

the remaining eigenvectors, which together explain <30% of the standardized parameter variance.

The correlations in Table 1a can be manipulated to produce linear regression relations to predict $\ln R_{\max}$, n , and X_I based upon knowledge of V_{\max} and \mathbf{n} .

$$R_{\max} = 46.4 \exp\{-0.0155V_{\max} + 0.0169\varphi\}, \quad (7.1)$$

$$X_I = 270.5 - 4.78V_{\max} + 6.176\varphi, \quad (7.2)$$

$$n = 0.431 + 0.136V_{\max} - 0.006\varphi. \quad (7.3)$$

All of the coefficients in (7.1-7.3) differ from zero with better than 1% statistical significance.

Substitution from (7.1-7.3) into (5) and continuation of the integral to large (1200 km) radius for incrementing values of maximum wind, produces a table of $(Z_e - Z_c)$ as a function of V_{\max} . Since an algebraic relation between minimum height and maximum wind is more useful than a table, we fit the tabular output with power-law expressions similar to that used by Atkinson and Holliday (1977). For example, at 25EN, the relation between minimum isobaric height and maximum wind is:

$$V_{\max} = 0.652(Z_e - Z_c)^{0.724}. \quad (8)$$

This relation takes into account the sharpening of the profile with intensity embodied in El ; whereas if one substitutes mean values of R_{\max} , n , X_I , and \mathbf{n} into (7.1-7.3), the profiles scale only as V_{\max} so that there is a “universal” height-wind relation with wind proportional to the square root of the height fall:

$$V_{\max} = 2.16\sqrt{Z_e - Z_c}. \quad (9)$$

In Part I, an empirical fit of maximum wind to height fall, yielded a similar relation with a coefficient of 2.10, based upon all the PCMP files---which includes the 113 profiles excluded here because they failed the QC criteria. The next section will deal more completely with the dynamically calculated height-wind relations for dual-exponential profiles.

As in Part I, bootstrap comparisons among subsets of the data provide an assessment of fitted profiles ability to represent independent data. The sample is divided into three subsets, spanning the years 1977-1989, 1990-1995, and 1996-2000, inclusive. Regression relations analogous to (7.1-7.3) were computed based upon all possible pairs of subsets and used to model the profiles in the subset excluded from each pair. In Part I, comparison of histograms of wind speed for both dependant and bootstrap data showed that the Holland profile exaggerated the occurrence of wind speeds $> 50 \text{ m s}^{-1}$ by 20-50%. The Holland profile also overstated the occurrence of winds $< 10 \text{ m s}^{-1}$ and understated that of winds between 20 and 40 m s^{-1} .

With dependant data (Fig 7a), in which the parameters are applied on a profile-by-profile basis to the data from which they were computed, the single-exponential profile also overestimates the occurrence of winds $> 40 \text{ m s}^{-1}$, but by $< 10\%$. For weaker winds, over and underestimation are mixed, with some preponderance of the latter. With dependant-data linear modeling of the parameters based upon all profiles that passed QC, the pattern is much the same, although occurrences of winds $> 70 \text{ m s}^{-1}$ and $< 10 \text{ m s}^{-1}$ are underestimated. Linearly modeled bootstrap parameters applied to the complete data set (Fig. 7b) are consistent with the dependant data results, but understate the occurrence of weak winds to a somewhat greater extent. Use of mean values of the parameters

greatly overstates the frequency of winds $> 40 \text{ m s}^{-1}$. Thus, while the sectionally continuous, single-exponential profile fixes some of the Holland profile's limitations, there is still room for improvement.

3. Dual-exponential profiles

Although the principle of least hypothesis makes the single-exponential profiles seem attractive, their tendency toward too-gradual radial decrease of wind with increasing radius just outside the eyewall and too rapid decrease at large radius, their systematic underestimation of the geopotential height fall from the vortex surroundings to center, and their overstating of the frequency of very strong and very weak winds, lead us to seek alternatives. The simplest option is inclusion of a second exponential in the outer vortex. Our original idea was to include a fixed slowly decaying exponential in order to flatten the profile at large radius and then to determine the faster decay length and its relative contribution with the fitting algorithm. The difficulty with this strategy lies in the ambiguous separation between the roles of the two exponentials in the cost-function minimization algorithm. Section 4 summarizes both this formulation and one where both decay lengths are determined variationally.

After some experimentation, we found that best version of (4) employed these outer-vortex parameters: X_2 , the fixed rapid decay length, X_1 , the fitted slower decay length, and A , the fitted contribution of the of the faster exponential to the profile. Subjective tuning showed that a wider transition, 25 km instead of 10 km, was required to avoid understating the frequency of the strongest winds with this formulation. Since smaller values of X_2 produced smaller rms differences between the observed and fitted wind profiles and smaller relative contributions by X_2 to the fitted profile, we selected the

most rapid decay length that seemed physically reasonable, 25 km, and applied a Lagrange multiplier constraint to keep $X_l > 100$ km. The upper bound on X_l was adjusted experimentally to bring the average value of $(Z_a - Z_e)$ close to zero (Fig. 8a). The value that met this criterion was $X_l < 450$ km. As the upper constraint on X_l relaxed, the average value increased (Fig 8b), but A remained essentially constant (Fig 8c). The average fitted values of n , X_l and A are 0.85, 288.5 km, and 0.10. The rms and bias wind and height differences between the fitted and observed profiles are 2.03 m s^{-1} , -0.07 m s^{-1} , 11.1 m, and 1.15 m. These values were relatively insensitive to the upper bound on X_l provided that it was > 400 km. Thus, use of two exponentials reduces the rms wind error by about 20% relative to the single exponential formulation, but reduces the wind bias and height errors by only a small amount. Because the faster decay length can fit the rapid decrease of wind speed outside the eyewall, the fitting algorithm usually selects larger value of X_l so that stronger winds extend farther from the center and integration of (5) to 1200 km radius produces zero average difference between the calculated and climatologically expected environmental geopotential height.

In only 167 of the cases that passed QC did the fitting algorithm select $A > 0$. In the other 326 cases—about 2/3 of the total— $A = 0$ produced the smallest S^2 so that the single exponential fit was superior to the dual-exponential fit. The average nonzero value of A was 0.26. Cyclones with nonzero A were stronger, average $V_{max} = 43.8 \text{ m s}^{-1}$, compared to those with $A = 0$, average $V_{max} = 33.1 \text{ m s}^{-1}$.

Despite the relatively small improvement in wind errors, the qualitative appearance of many fitted profiles was more realistic. In Hurricane Anita, where the algorithm selected $X_l = 301$ km and $A = 0.41$, the fitted and observed profiles are

virtually identical (Fig. 9); whereas the single exponential fit with $X_I = 100$ km was only slightly better than the corresponding Holland fit. For Hurricane Mitch (Fig 10a), the dual exponential fit selected $X_I = 156$ km and $A = 0.14$. The new X_I was only 30% larger than the corresponding single-exponential value, but the dual-exponential fit was noticeably better beyond 40 km radius. In both Hugo (Fig. 10b) and Edouard (Fig. 10c), the fitting algorithm chose $A = 0$. The single exponential fit was optimum in these cyclones and the fitted profiles were identical to those shown in Fig. 5, apart from the effect of the wider transition zone. For Erika (Fig. 10c), the algorithm again chose a relatively small value of $A = 0.13$, and a relatively larger value of $X_I = 318$ km, approximately double the single-exponential value in Fig. 5. Figures 9 and 10 are typical of the dual-exponential fits. For some hurricanes, generally those with $V_{\max} > 55 \text{ m s}^{-1}$, nonzero values of A produce substantially more realistic fits. For some weaker hurricanes values of A between the sample average and zero produce incremental improvements. A key advantage of this formulation is that the fitting algorithm can select $A = 0$ for cyclones where the single-exponential fit is optimum, as illustrated for Hugo and Edouard.

Scatter diagrams of A , X_I , and n as functions of V_{\max} are consistent with this interpretation. Values on a regression line fitted to X_I decrease from 352 km to 211 km as V_{\max} increases from 5 to 75 m s^{-1} . Although few values of X_I are limited by the Lagrange multiplier minimum constraint $100 \text{ km} \leq X_I$, ~25% of them cluster along the maximum constraint $X_I \leq 450$ km (Fig. 11a). The reason for this difference from the single-exponential case (Fig. 6) lies the tighter constraint and the dual-exponential profiles' ability to represent sharp gradients near the eyewall with the X_2 part of the profile while representing the outer vortex with larger values of X_I . Nonzero values of A correspond to

partial projection onto the X_2 component. The regression line for this parameter is not allowed to extend to negative values so that $A = 0$ for $V_{\max} \leq 20 \text{ m s}^{-1}$ and increases to 0.29 at $V_{\max} = 75 \text{ m s}^{-1}$. Still, in roughly two-thirds of the sorties, $A \simeq 0$, so that the single-exponential profile is actually the optimum fit, as discussed above and illustrated in Figs. 9 and 10. The exponent of the power-law profile inside the eye is a bit larger than in the single-exponential profile because of the wider transition region. Only about 4% of the values are greater than two.

The parameter correlation matrix (Table 2a) is for the most part consistent with that for the single-exponential and Holland profiles. Here, A , X_1 , and n play the same role as B in the Holland profile. The leading eigenvector, which explains $> 40\%$ of the standardized parameter variance, is the same as the one recognized in the previous situations. It describes sharpening of the wind maximum and shrinking of the radius of maximum wind in more intense tropical cyclones---the convective ring phenomenon. This eigenvector has a larger eigenvalue than the corresponding single-exponential eigenvector, but it explains less of the variance because the total standardized parameter variance is 6 instead of 5. A key difference between the single- and dual-exponential profiles is the stronger projection of this eigenvector onto A and n compared with X_1 . The second eigenvector describes simultaneous reduction in X_1 and A associated (weakly) with increasing intensity. It may reflect the non-uniqueness inherent in approximation of curves by sums of exponentials. That is, a smaller variable decay length with less contribution from the fixed decay length may fit a given profile just as well as a larger variable decay length with more contribution from the fixed exponential. The third eigenvector is the same as the second eigenvector identified in the Holland and single-

exponential cases. It projects almost entirely onto latitude. Together, these first three eigenvectors explain nearly 80% of the parameters' standardized variance.

As in the single-exponential case, the correlations in Table 2a yield linear regression relations to predict $\ln R_{\max}$, n , X_l and A based upon knowledge of the variables that characterize hurricanes in the HURDAT file, V_{\max} and \boldsymbol{n} . Since the regression relation for R_{\max} is identical with (7.1), it is not repeated here

$$X_l = 317.1 - 2.026V_{\max} + 1.915\varphi, \quad (10.1)$$

$$n = 0.4067 + 0.0144V_{\max} - 0.0038\varphi, \quad (10.2)$$

$$A = 0.0696 + 0.0049V_{\max} - 0.0064\varphi, \quad (A \geq 0), \quad (10.3)$$

The coefficients in (10.1-10.3) differ from zero at better than 1% significance, except for the last (φ) coefficients in 10.1 and 10.2, which are significant at 1.4% and 16%, respectively. Alternative regression relations that use radius of maximum wind as an independent variable in addition to maximum wind and latitude are:

$$X_l = 287.6 - 1.942V_{\max} + 7.799\ln R_{\max} + 1.819\varphi, \quad (11.1)$$

$$n = 2.1340 + 0.0077V_{\max} - 0.4522\ln R_{\max} - 0.0038\varphi, \quad (11.2)$$

$$A = 0.5913 + 0.0029V_{\max} - 0.1361\ln R_{\max} - 0.0042\varphi, \quad (A \geq 0). \quad (11.3)$$

As above, all of the coefficients differ from zero at better than 1%, except for the next-to-last coefficient ($\ln R_{\max}$) in (11.1), 50%, and the last (φ) coefficients in (11.1) and (11.2), 2.5% and 8.5%, respectively. The coefficients are so different between these two sets of equations because in (10.1-10.3) variations of the dependant variables that would project onto $\ln R_{\max}$ ---if it were an independent variable--- project instead onto V_{\max} and \boldsymbol{n} through their correlations with $\ln R_{\max}$.

Here we treat in more detail derivation of height-wind relations based upon the regression relations for the parameters. As in Section 2, substitution from (10.1-10.3) into (5) and integrating to 1200 km radius produces $Z_e - Z_c$ a function of V_{\max} . Algebraic relations between minimum height and maximum wind are derived by fitting power-law expressions to the resulting tabular data:

$$V_{\max} = 0.929 (Z_e - Z_c)^{0.659}, \quad (\varphi = 15^\circ \text{N}), \quad (12.1)$$

$$V_{\max} = 0.661 (Z_e - Z_c)^{0.701}, \quad (\varphi = 25^\circ \text{N}), \quad (12.2)$$

$$V_{\max} = 0.508 (Z_e - Z_c)^{0.730}, \quad (\varphi = 35^\circ \text{N}), \quad (12.3)$$

$$V_{\max} = 0.410 (Z_e - Z_c)^{0.752}, \quad (\varphi = 45^\circ \text{N}), \quad (12.4)$$

$$V_{\max} = 2.20 \sqrt{Z_e - Z_c}, \quad (\text{mean ln } R_{\max}, \mathbf{n}, n, X_I \text{ and } A). \quad (12.5).$$

Although the coefficients in these relations vary considerably, the actual values are surprisingly consistent, both with each other and with observed V_{\max} as a function of $Z_e - Z_c$ (Fig, 12). The mean and rms errors with (12.1-12.4) using data stratified by 10° latitude bands are $0.85 \pm 5.92 \text{ m s}^{-1}$. With the pooled-data square-root relationship the error is $1.48 \pm 5.87 \text{ m s}^{-1}$. These errors are essentially the same as those with the dependant-data height wind relations fitted to the complete data set in Part I. Not surprisingly, (12.5), the mean-parameter height wind relation overestimates the maximum wind in weaker tropical cyclones and underestimates it in stronger ones because it fails to account for the statistical sharpening of the profile with intensity. The scatter of the actual maximum winds as a function of height difference is greater than can be accounted for by latitude differences in (12.1-12.4), and much of it is due to random variations of the parameters not captured by the regression relations. The errors from (12.1-12.4) are

significantly smaller than the corresponding errors with the Holland profile using linearly estimated B in Part I, $-2.53 \pm 6.48 \text{ m s}^{-1}$. From the combined analysis here and in Part I, it appears difficult to derive a height-wind relationship that can estimate maximum wind with an rms error appreciably smaller than 6 m s^{-1} .

Dependant-data histograms of the observed and fitted-profile winds show gratifying agreement (Fig. 13a) using both profile-specific parameters and linearly estimated parameters. The only noticeable problems are overstatement of the frequency of winds between 60 and 70 m s^{-1} and understating the frequency of winds between 70 and 80 m s^{-1} by $\sim 10\%$. Bootstrap validation with linearly estimated parameters (Fig. 13b) increases the overestimation of wind occurrence in the $60\text{-}70 \text{ m s}^{-1}$ bin, causes underestimation in the $< 10 \text{ m s}^{-1}$ bin, and reduces the error in the $70\text{-}80 \text{ m s}^{-1}$ bin. Consistent with the Holland and single-exponential experience, average values of the parameters overestimate occurrences on both the high- and low-speed tails of the wind distribution.

4. Discussion

a. Other formulations

Two other ways to fit dual exponentials to the outer-profile data involve setting X_2 to a fixed value of $300\text{-}500 \text{ km}$ and searching variationally for A and X_1 with the latter parameter limited to values $< 25\text{-}150 \text{ km}$. This approach has 5 parameters, the same number as in Section 3. Alternatively, both X_1 and X_2 may be sought through a free dual-exponential variational search. This approach has a total of 6 parameters: V_{\max} , R_{\max} , n , X_1 , A , and X_2 , four of which must be sought with the fitting algorithm. Both of these approaches are compromised by the proliferation of potentially spurious correlations

among parameters and the multiple ways that different combinations of parameters can fit the same data equally well.

Figure 14 shows scatter diagrams of the free dual-exponential outer-vortex parameters with Lagrange multiplier constraints $100 \leq X_1 \leq 450$ and $25 \leq X_2 \leq 75$ km. The regression relation for X_1 behaves much as it did in Section 3, decreasing from > 300 km to < 200 km as V_{\max} increases from 5 to 75 m s^{-1} (Fig 14a). About 14 % of values are limited by the 450 m s^{-1} upper Lagrange multiplier constraint, and unlike the analysis in Section 3, about 2% are limited by the lower constraint. A on the other hand behaves differently (Fig 14b). Only 55% of the values are zero, implying that here single exponential fits are optimum in somewhat fewer cases than previously. The algorithm also produces $\sim 2\%$ of cases with $A = 1$, implying that in those case X_2 , which is constrained within the domain $25 \leq X_2 \leq 75$ km, can completely describe the vortex outside the eye. Despite the lack of a consistent pattern in the dual-exponential fit, its regression relation for A is similar to that for the dual exponential fit with fixed $X_2 = 25$ km, but without the identically zero values when the previous regression line was negative for $V_{\max} < 20 \text{ m s}^{-1}$. The X_2 scatter diagram shows erratic variation. About 47% of the X_2 values are at the lower Lagrange multiplier limit, 25 km, so that the fits to these profiles are the same as in Section 3. Another 18% of the X_2 values are > 75 km where they are significantly penalized by the upper X_2 constraint. These instances reflect ambiguity as the roles of the longer and shorter decay lengths overlap.

As a consequence, the regression line describes X_2 as a constant value of ~ 45 km, independent of V_{\max} . Despite the additional degrees of freedom, the free dual-exponential fit has larger rms wind and height errors, 2.81 m s^{-1} and 12.20 m , compared with 2.03

m s^{-1} and 11.06 m in with X_2 fixed at 25 m s^{-1} . A similarly vexing ambiguity problem arises with the shorter decay length when one attempts to fit it, A , and a fixed longer decay length. The reason for these problems lies in local minima of the cost-function that are distinct from the global minimum. Perhaps insightful application of different constraints and a more sophisticated minimization algorithm can resolve these issues, but for now, the dual exponential profile with a fixed shorter decay length seems to be the simplest representation of the data.

b. Vortex stability

Since one potential application of these profiles is theoretical studies of vortex dynamics, it is useful to explore their hydrodynamic stability properties. Figure 15 shows the absolute vorticity and angular velocity for the dual-exponential profile fitted to Hurricane Anita (Fig. 9). The vorticity is everywhere > 0 so that the profile is inertially stable. It exhibits a relative minimum at the center and a pronounced maximum just inside the radius the radius of maximum wind so that it meets the necessary condition for barotropic instability (e.g. Schubert et al. 1999). The vortex angular velocity also exhibits a maximum that causes the algebraically growing wavenumber-one instability described by Nolan and Montgomery (2000). The vorticity and angular velocity maxima in Anita arise partly because $n > 1$, but the way that the outer and inner profiles overlap in the transition zone generally produces local maxima of these quantities near the eyewall even when $n < 1$. In that case, the profile would have infinite angular velocity and vorticity at the center if it were continued to $r = 0$. Difficulty with the singularity can be avoided in these cases either by insertion of a patch of constant vorticity around the center or by simply not computing vorticity or angular velocity at the center point.

5. Conclusions

The dual-exponential profiles presented here provide an observationally-based representation of the structure of the hurricane vortex to support such diverse undertakings as theoretical vortex dynamics, storm-surge forecasting, and windstorm loss modeling. The statistical estimates of the parameters given by (7.1, 10.1-10.3 and 11.1-11.3) allow construction of axisymmetric hurricane vortices using (1.1-1.3 and 4). The resulting wind variations are consistent with a large sample of aircraft observations and have latitude-dependant height-wind relations (12.1-12.4). Although these relations take into account the statistical sharpening of the wind maximum in more intense tropical cyclones, maximum winds computed from them have an inherent uncertainty of $\sim 6 \text{ m s}^{-1}$.

A key limitation of this study is exclusion of tropical cyclones that failed to meet the QC criteria because they had large radii of maximum wind. Reanalysis including hurricane that have occurred since the 2000 season, and using different QC criteria and different Lagrange multiplier constraints promises to improve this situation. Other unfinished work is calibration of the axisymmetric maximum wind in terms of the HURDAT climatology and inclusion of secondary wind maxima in the statistical representation.

Acknowledgements: Our coauthor, Ed Rahn, died in November 2004 as we were finalizing this paper. His meticulous analysis of aircraft data and formidable programming talent were cornerstones of this work. He was a good friend and colleague who will be missed.

We are grateful to scientists, flight crew and ground support staff in NOAA and the Air Force. Without their skill and dedication in difficult and demanding conditions,

this research would have been impossible. The acquisition and maintenance of the data archive was supported by Hurricane Research Division base funds, and HEW's efforts since December 2002 were supported by Florida International University research discretionary funds. We thank Sneh Gulati for statistical advice.

APPENDIX: BELLRAMP FUNCTIONS

In Section 2, the transition between the outer exponential profile and the inner power-law profile was accomplished with a polynomial that superficially resembled a hyperbolic tangent, but had finite width and increased smoothly from zero to one as its nondimensional argument, \mathfrak{z} , also increased from zero to one. This polynomial “ramp function” was derived by integration of a polynomial “bell function” of the form:

$$b_k(\xi) = 0, \quad (\xi \leq 0 \text{ or } 1 \leq \xi), \quad (\text{A1.1})$$

$$b_k(\xi) = C_k [\xi(1-\xi)]^k, \quad (0 \leq \xi \leq 1). \quad (\text{A1.2})$$

Here k is the order of the bell function, although b_k is a polynomial of order $2k$. The $k/1^{\text{st}}$ derivative of b_k is highest derivative that remains continuous at $\xi = 0$ and $\xi = 1$. Thus, for b_1 only the function itself is continuous; for b_2 the function and first derivative are continuous, and so forth. As shown below, the bell curves become narrower with increasing order. $[\xi(1-\xi)]^k$ has maximum value on $(0 \leq \xi \leq 1)$ of 2^{-2k} at $\mathfrak{z} = 1/2$ so that setting $C_k = 2^{2k}$ would produce bell functions with unit amplitude.

A more interesting alternative involves integration of b_k from zero to one and selection of C_k to make the area under the bell curve unity. Here are the $k = 1$ through 4 ramp functions produced by integration of $b_1(\mathfrak{z})$ through $b_4(\mathfrak{z})$ in a form convenient for numerical calculation and accompanied by the coefficient needed to make $w_k(1) = 1$:

$$w_1(\xi) = C_1 \xi^2 (3 - 2\xi), \quad C_1 = 6, \quad (\text{A2.1})$$

$$w_2(\xi) = C_2 \xi^3 (10 - \xi(15 - 6\xi)), \quad C_2 = 30, \quad (\text{A2.2})$$

$$w_3(\xi) = C_3 \xi^4 (35 - \xi(84 - \xi(70 - 20\xi))), \quad C_3 = 140, \quad (\text{A2.3})$$

$$w_4(\xi) = C_4 \xi^5 (126 - \xi(420 - \xi(540 - \xi(315 - 70\xi)))), \quad C_4 = 630. \quad (\text{A2.4})$$

By definition, $w_k(\xi) = 0$ when $\xi \leq 0$, and $w_k(\xi) = 1$ when $1 \leq \xi$.

Figures A1a and A1b illustrate $b_1(\xi)$ through $b_4(\xi)$ and $w_1(\xi)$ through $w_4(\xi)$, respectively. As anticipated, the bell curves become narrower, and their amplitude increases with increasing k while the transition described by w_k becomes sharper. Some of these polynomials are familiar in other contexts. For example, (A2.1) is a Hermite shape function used in finite-element analysis. In the limit of very large k , b_k and w_k respectively approach Dirac delta and Heaviside functions, albeit gradually. Thus, it is possible to produce highly differentiable finite-width bell and ramp curves by the method outlined here. Because these curves are efficient to compute, they offer simple-to-use alternatives to Gaussian or hyperbolic-tangents functions for constructing forcing functions for theoretical models, representation of jet or shear flows, or patching together piecewise continuous curves as we have done here.

REFERENCES

- Atkinson, G. D. and C. R. Holliday, 1977: Tropical cyclone minimum sea-level pressure/maximum sustained wind relationship for the western North Pacific. *Mon. Wea. Rev.*, **105**, 421-427.
- Holland, G. J., 1980: An analytic model of the wind and pressure profiles in hurricanes. *Mon. Wea. Rev.*, **108**, 1212-1218.
- Jarvinen, B. R., C. J. Neumann, and M. A. S. Davis, 1984: A tropical cyclone data tape for the North Atlantic Basin, 1886-1983: Contents, limitations, and uses. NOAA Technical Memorandum, NWS NHC 22, Coral Gables, Florida, 21 pp
[<http://www.nhc.noaa.gov/pastall.shtml>].
- Jelesnianski, C. P., 1967: Numerical computation of storm surges with bottom stress. *Mon. Wea. Rev.*, **95**, 740-756.
- Jordan, C. L., 1958: Mean soundings for the West Indies area. *J. Meteor.*, **15**, 91-97.
- Nelder, J. A. and R. Mead, 1965: A simplex method for function minimization. *The Computer Journal*, **7**, 308-313
- Nolan, D. S., and M. T. Montgomery, 2000: The algebraic growth of wavenumber one disturbances in hurricane-like vortices. *J. Atmos. Sci.*, **57**, 3514-3538.
- Press, W. H., B. P. Flannery, S. A. Teukolsky, and W. T. Vetterling, 1986: 10.4 Downhill simplex method in multidimensions, *Numerical Recipes, The Art of Scientific Computing*, Cambridge University Press, 289-293.
- Schubert, W. H. and J. J. Hack, 1982: Inertial stability and tropical cyclone development, *J. Atmos. Sci.*, **39**, 1687-1697.

- Schubert, W. H., M. T. Montgomery, R. K. Taft, T. A. Guinn, S. R. Fulton, J. P. Kossin, J. P. Edwards, 1999: Polygonal eyewalls, asymmetric eye contraction and potential vorticity mixing in hurricanes. *J. Atmos. Sci.*, **56**, 1197-1223.
- Shapiro, L. J., and H. E. Willoughby, 1982: The response of balanced hurricanes to local sources of heat and momentum, *J. Atmos. Sci.*, **39**, 378-394.
- Sheets, R. C.: 1969: Some mean hurricane soundings. *J. Appl. Meteor.*, **8**, 134-146.
- Smith, R. K., 1981: The cyclostrophic adjustment of vortices with application to tropical cyclone modification, *J. Atmos. Sci.*, **38**, 2021-2030.
- Vickery, P. J., and L. A. Twisdale, 1995: Prediction of hurricane wind speeds in the United States. *J. Struct. Eng.*, **121**, 1691-1699.
- Willoughby, H. E., 1995: Normal-mode initialization of barotropic vortex motion models. *J. Atmos. Sci.*, **52**, 4501-4514.
- Willoughby, H. E. and M. E. Rahn, 2004: Parametric representation of the primary hurricane vortex. Part I: Observations and evaluation of the Holland (1980) model. *Mon. Wea. Rev.*, **132**, 3033-3048.

TABLES CAPTIONS

Table 1. (a.) Mean, standard deviation and correlation matrix for the single-exponential profile variables computed from the 493 sorties that passed QC screening. For R_{max} the entries are the geometric mean in kilometers and the logarithmic standard deviation. (b.) Eigenvalues and eigenvectors of the correlation matrix.

Table 2 (a.) Mean, standard deviation and correlation matrix for the dual-exponential profile variables computed with X_2 fixed at 25 km from the 493 sorties that passed QC screening. For R_{max} the entries are the geometric mean in kilometers and the logarithmic standard deviation. (b.) Eigenvalues and eigenvectors of the correlation matrix.

TABLES

Table 1. (a.) Mean, standard deviation and correlation matrix for the single-exponential profile variables computed from the 493 sorties that passed QC screening. For R_{max} the entries are the geometric mean in kilometers and the logarithmic standard deviation. (b.) Eigenvalues and eigenvectors of the correlation matrix.

(a.)	Distribution		Correlation Matrix				
	Mean	SD	Z_1	Z_2	Z_3	Z_4	Z_5
$Z_1(V_{max})$	36.7	13.7	1.000	-0.398	-0.018	-0.468	0.561
$Z_2(\ln R_{max})$	39.3	0.53	-0.398	1.000	0.200	0.454	-0.602
$Z_3(\varphi)$	23.9	6.15	-0.018	0.200	1.000	0.278	-0.115
$Z_4(X_I)$	242.9	141.3	-0.468	0.454	0.278	1.000	-0.424
$Z_5(n)$	0.79	0.34	0.561	-0.602	-0.115	-0.424	1.000

(b.) Eigenvector	$E1$	$E2$	$E3$	$E4$	$E5$
Eigenvalue	2.518	1.026	0.625	0.495	0.335
$Z_1(V_{max})$	0.470	-0.346	-0.450	0.505	-0.449
$Z_2(\ln R_{max})$	-0.497	-0.012	-0.598	0.372	0.507
$Z_3(\varphi)$	-0.197	-0.896	-0.014	-0.392	0.057
$Z_4(X_I)$	-0.474	-0.184	0.565	0.602	-0.244
$Z_5(n)$	0.518	-0.207	0.346	0.300	0.692

Table 2 (a.) Mean, standard deviation and correlation matrix for the dual-exponential profile variables computed with X_2 fixed at 25 km from the 493 sorties that passed QC screening. For R_{max} the entries are the geometric mean in kilometers and the logarithmic standard deviation. (b.) Eigenvalues and eigenvectors of the correlation matrix.

(a.)	Distribution		Correlation Matrix					
	Mean	SD	Z_1	Z_2	Z_3	Z_4	Z_5	Z_6
$Z_1(V_{max})$	36.7	13.7	1.000	-0.398	-0.018	-0.254	0.479	0.421
$Z_2(\ln R_{max})$	39.3	0.53	-0.398	1.000	0.200	0.152	-0.667	-0.572
$Z_3(\varphi)$	23.9	6.15	-0.018	0.200	1.000	0.112	-0.065	-0.251
$Z_4(X_1)$	288.5	112.0	-0.254	0.152	0.112	1.000	-0.143	0.165
$Z_5(n)$	0.85	0.42	0.479	-0.667	-0.065	-0.143	1.000	0.391
$Z_6(A)$	0.10	0.16	0.421	-0.572	-0.251	0.165	0.391	1.000

(b.) Eigenvector	$E1$	$E2$	$E3$	$E4$	$E5$	$E6$
Eigenvalue	2.550	1.150	1.022	0.625	0.417	0.235
$Z_1(V_{max})$	-0.443	0.246	-0.239	0.700	-0.324	0.302
$Z_2(\ln R_{max})$	0.536	0.054	-0.003	0.432	-0.348	-0.663
$Z_3(\varphi)$	0.180	0.150	-0.907	-0.066	0.338	-0.061
$Z_4(X_1)$	0.135	-0.835	-0.270	0.001	-0.382	0.255
$Z_5(n)$	-0.504	0.087	-0.214	-0.466	-0.520	-0.451
$Z_6(A)$	-0.460	-0.457	0.027	0.317	0.493	-0.484

FIGURES

1. (a.) Schematic illustration of a sectionally continuous hurricane wind profile constructed by joining an inner profile with swirling wind proportional to a power of radius and an outer profile with swirling wind decaying exponentially with distance outside the radius of maximum wind. In a zone spanning the radius of maximum wind, a polynomial ramp weighting function (b.) is used to create a smooth transition between the inner and outer profiles.
2. A dual-exponential profile used to approximate the observed wind in Hurricane Diana on 11 September 1984.
3. Variation of (a.) outer exponential decay length and (b.) difference between computed and climatological environmental geopotential heights as a function of the Lagrange-multiplier constraint on the maximum decay length for single-exponential profiles.
4. Single-exponential (a.) wind and (b.) geopotential height profiles fitted to Hurricane Anita of 1977.
5. Single-exponential wind profiles fitted to Hurricanes (a.) Mitch of 1998, (b.) Hugo of 1989, (c.) Edouard of 1996, and (d.) Erika of 1997.
6. Scatter plots and regression lines for fitted (a.) single-exponential outer decay length and (b.) power-law exponent as functions of maximum wind. Shaded circles represent parameter values determined for individual profiles by the fitting algorithm.
7. Histograms of observed and single-exponential profile wind speeds: (a.) Dependant-data observed (gray), computed from profile-specific fitted parameters

- (cross-hatched), and computed from linearly estimated parameters for profiles that passed QC (black). (b.) Complete-sample observed (gray), computed from linearly estimated parameters (cross-hatched), and computed from sample mean parameters (black). Both panels use observed radius of maximum wind.
8. Variation of (a.) difference between computed and climatological environmental geopotential heights, (b) outer exponential decay length and (c.) fraction of the profile contributed by the shorter exponential with 25 km decay length as functions of the Lagrange-multiplier constraint on the maximum longer decay length for dual-exponential profiles.
 9. Dual-exponential (a.) wind and (b.) geopotential height profiles fitted to Hurricane Anita of 1977.
 10. Dual-exponential wind profiles fitted to Hurricanes (a.) Mitch of 1998, (b.) Hugo of 1989, (c.) Edouard of 1996, and (d.) Erika of 1997.
 11. Scatter plots and regression lines as functions of maximum wind for fitted (a.) dual-exponential longer (solid) and shorter (dashed, fixed at 25 km) decay lengths, (b.) fraction that the shorter decay length contributes to the outer profile, and (c.) inner vortex power-law exponent. Shaded circles represent parameters values determined by the fitting algorithm.
 12. Height-wind relation computed from the dual-exponential profiles. Shaded circles represent observed wind speed as a function of the difference between climatological environmental geopotential height and observed central geopotential height. Dashed curves are power-law approximations (12.1-12.4) to the height difference computed from the gradient-wind relation using parameters

- estimated linearly from maximum wind and latitude at 15E, 25E, 35E, and 45E latitude. The solid curve is the height-wind relation (12.5) computed with the sample-mean values of the parameters.
13. Histograms of observed and dual-exponential profile with $X_2 = 25$ km wind speeds: (a.) Dependant-data observed (gray), computed from profile-specific fitted parameters (cross-hatched), and computed from linearly estimated parameters for profiles that passed QC (black). (b.) Complete-sample observed (gray), computed from linearly estimated parameters (cross-hatched), and computed from sample mean parameters (black). Both panels use observed radius of maximum wind.
14. Scatter plots and regression lines as functions of maximum wind for fitted (a.) free, dual-exponential, longer decay length, (b.) fraction that the shorter decay length contributes to the outer profile and (c.) free, dual-exponential, shorter decay length. Shaded circles represent parameter values determined by the fitting algorithm.
15. Vorticity (solid) and angular velocity (dashed) for the dual-exponential profile with $X_2 = 25$ km fitted to Hurricane Anita of 1977, thin line separating white and gray areas.
- A1. Polynomial bell and ramp functions computed from (A1) and (A2).

Sectionally Continuous Wind Profile

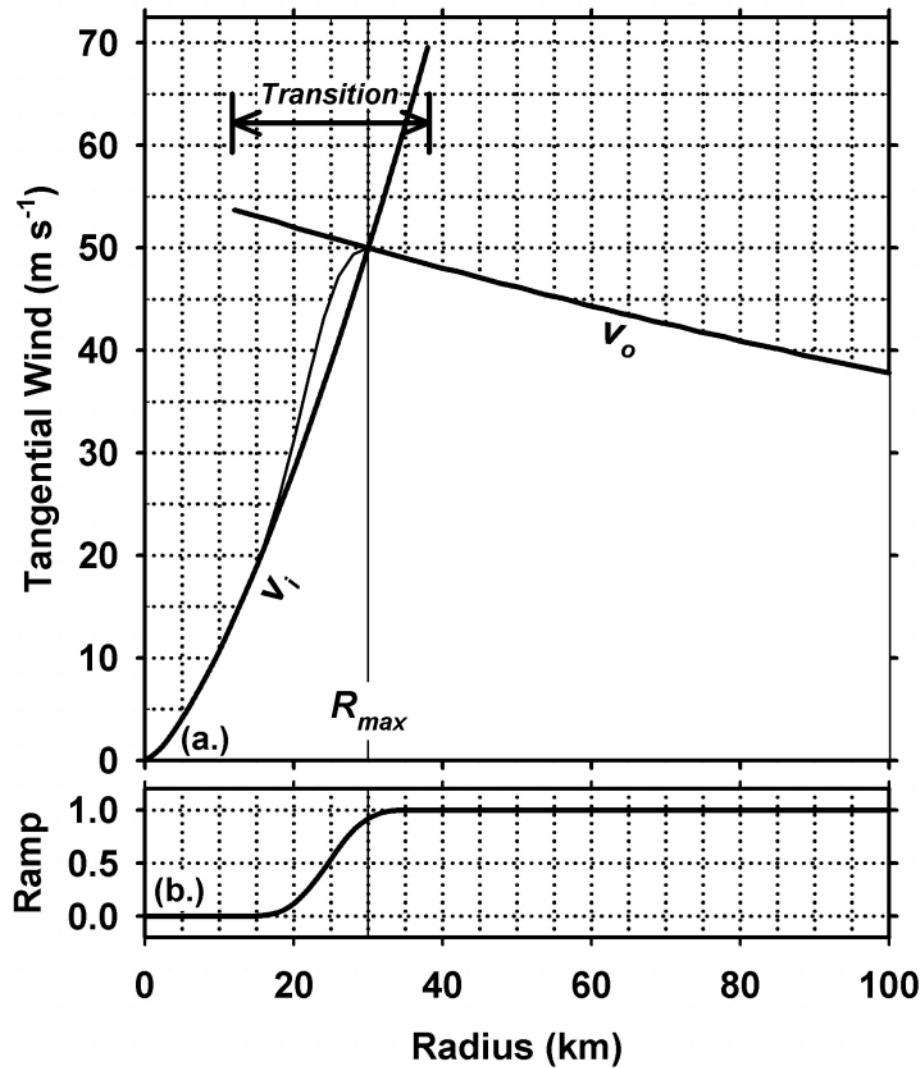


Fig. 1. (a.) Schematic illustration of a sectionally continuous hurricane wind profile constructed by joining an inner profile with swirling wind proportional to a power of radius and an outer profile with swirling wind decaying exponentially with distance outside the radius of maximum wind. In a zone spanning the radius of maximum wind, a polynomial ramp weighting function (b.) is used to create a smooth transition between the inner and outer profiles.

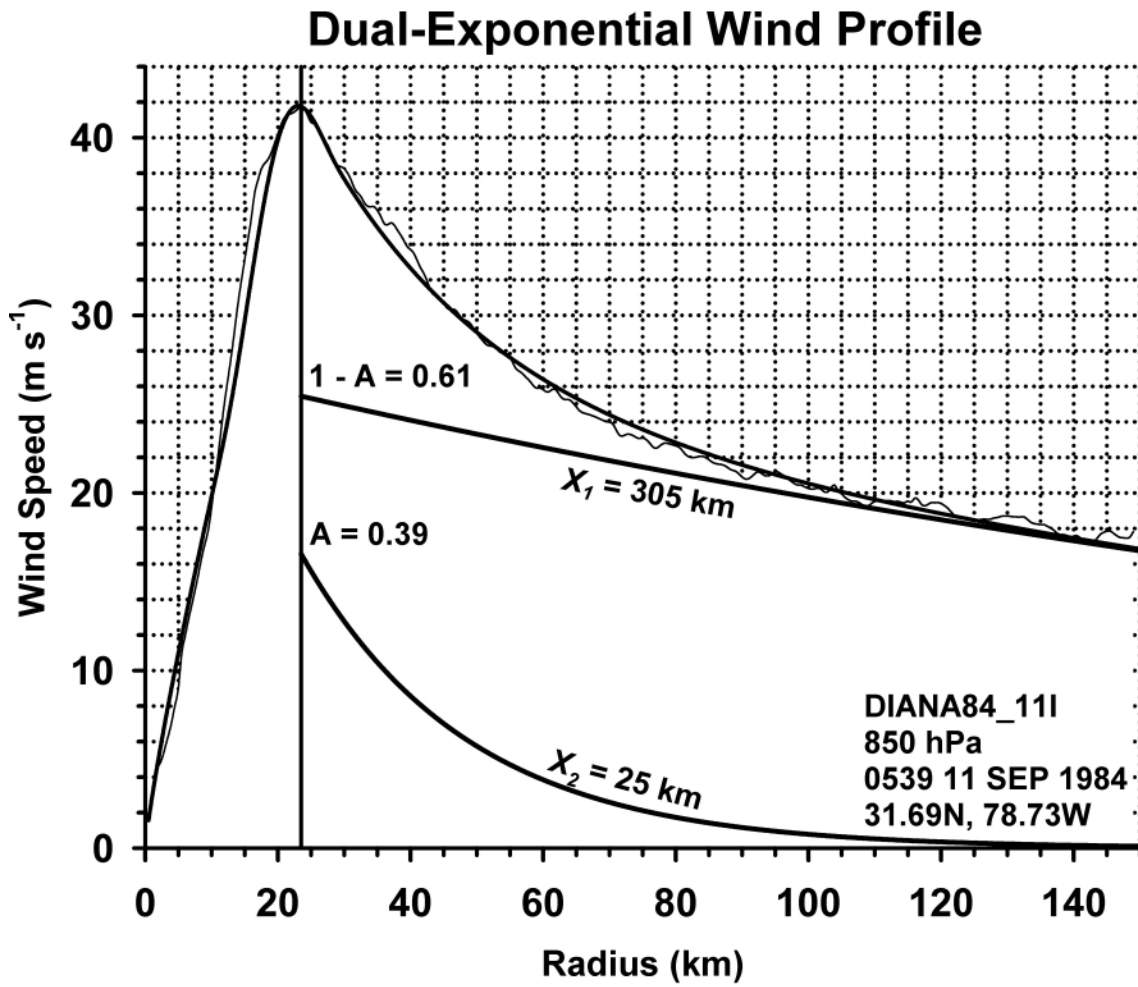


Fig. 2. A dual-exponential profile used to approximate the observed wind in Hurricane Diana on 11 September 1984.

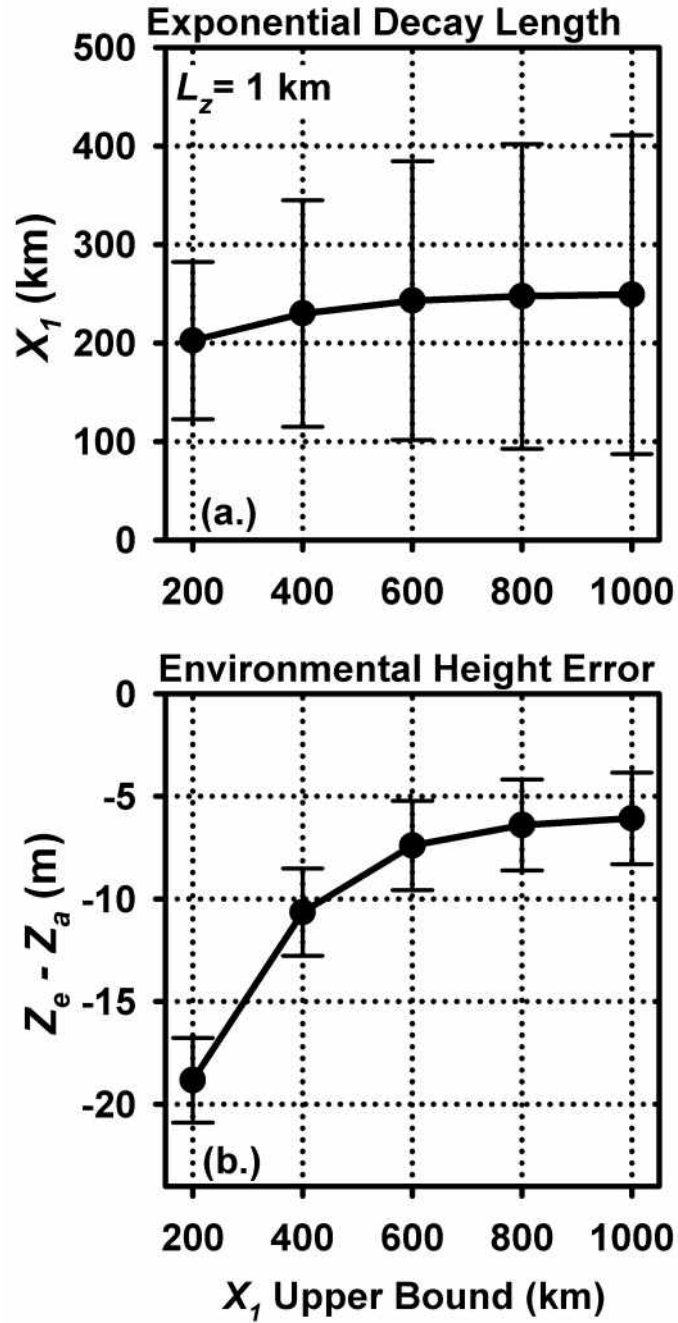


Fig. 3. Variation of (a.) outer exponential decay length and (b.) difference between computed and climatological environmental geopotential heights as a function of the Lagrange-multiplier constraint on the maximum decay length for single-exponential profiles.

ANITA77_01H

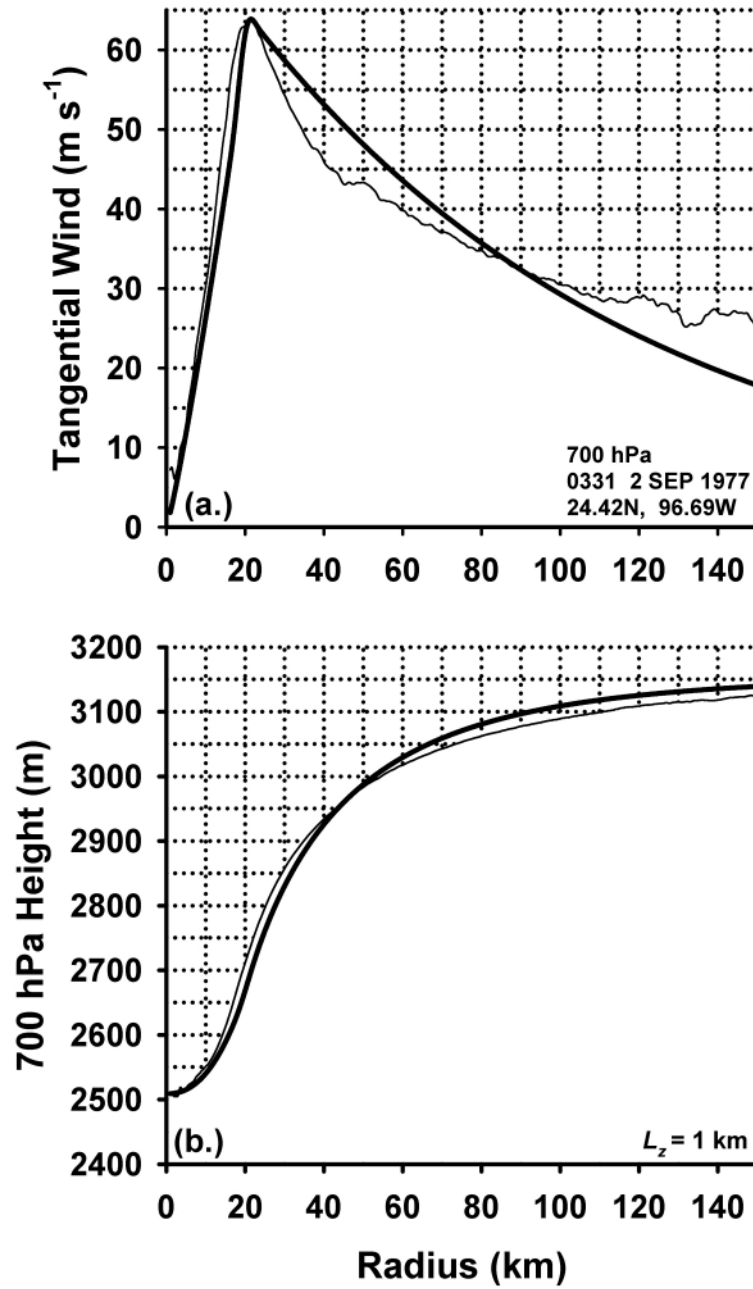


Fig. 4. Single-exponential (a.) wind and (b.) geopotential height profiles fitted to Hurricane Anita of 1977.

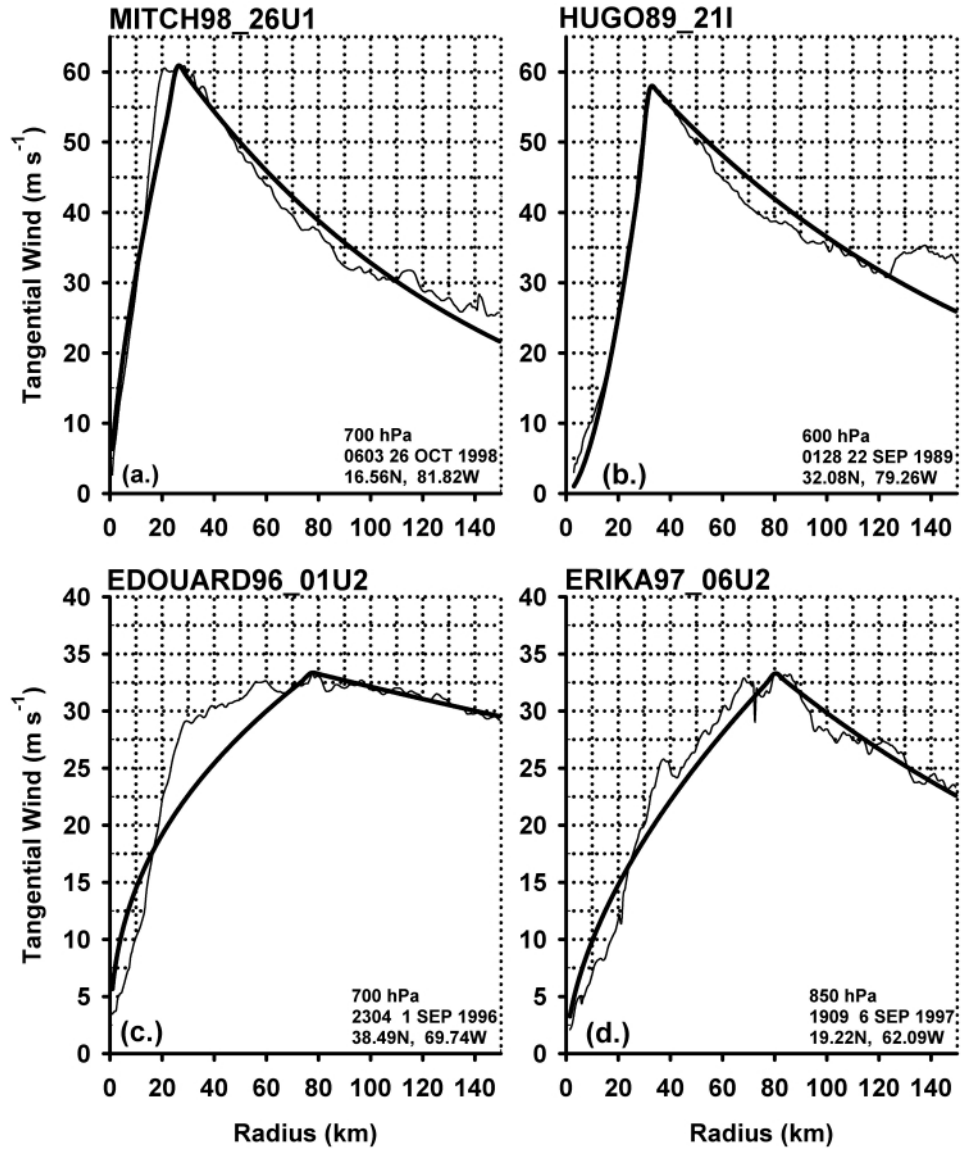


Fig. 5. Single-exponential wind profiles fitted to Hurricanes (a.) Mitch of 1998, (b.) Hugo of 1989, (c.) Edouard of 1996, and (d.) Erika of 1997.

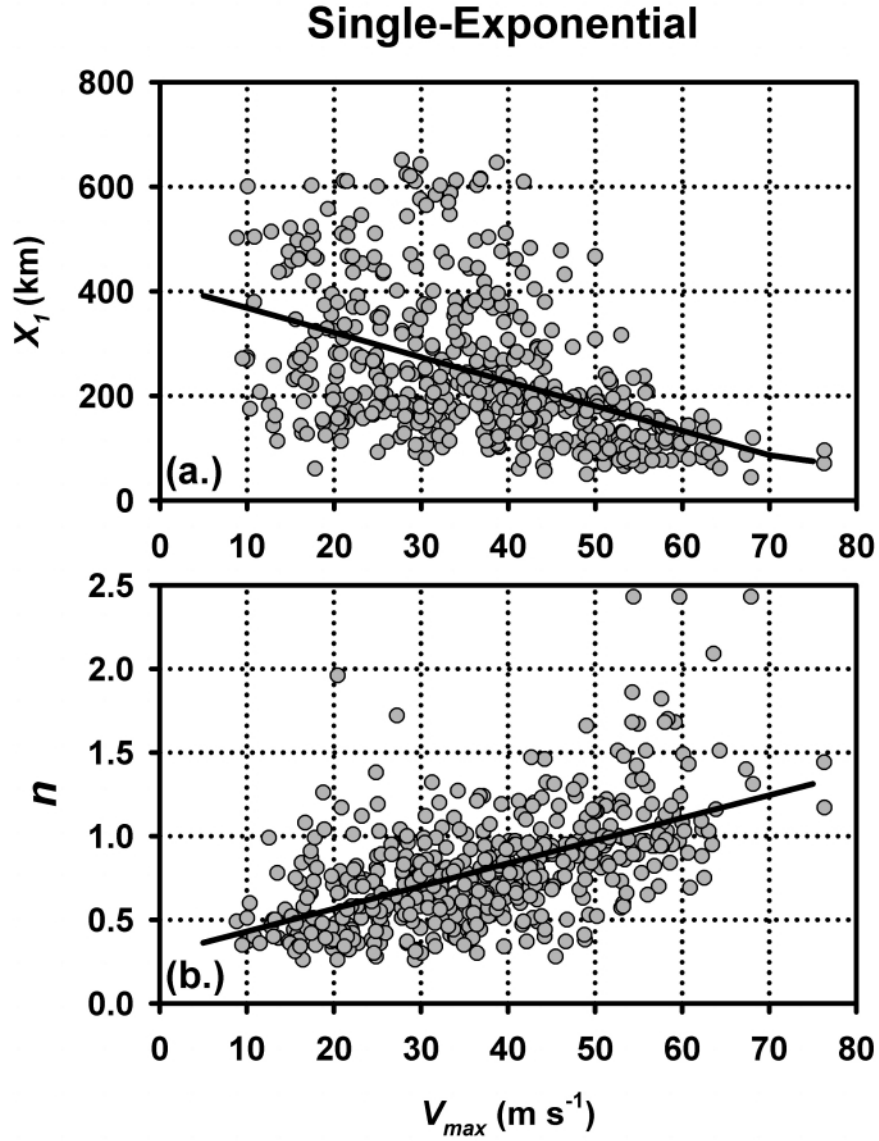


Fig. 6. Scatter plots and regression lines for fitted (a.) single-exponential outer decay length and (b.) power-law exponent as functions of maximum wind. Shaded circles represent parameter values determined for individual profiles by the fitting algorithm.

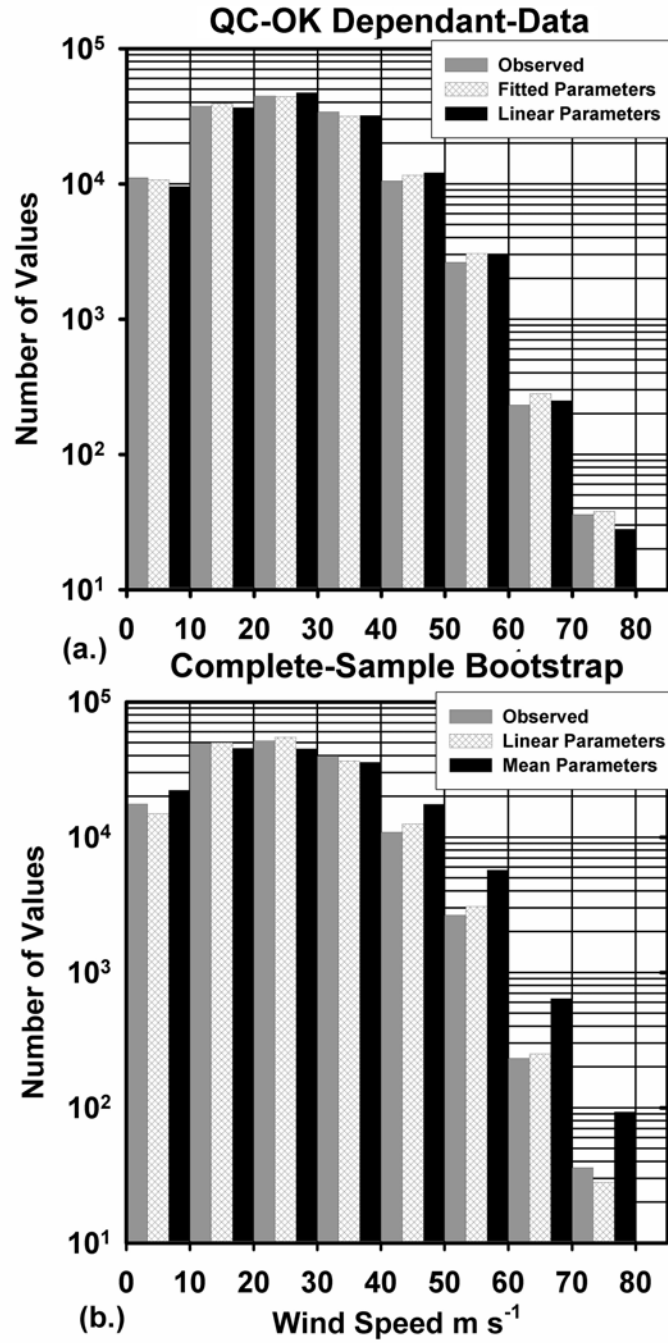


Fig. 7. Histograms of observed and single-exponential profile wind speeds: (a.) Dependant-data observed (gray), computed from profile-specific fitted parameters (cross-hatched), and computed from linearly estimated parameters for profiles that passed QC (black). (b.) Complete-sample observed (gray), computed from linearly estimated parameters (cross-hatched), and computed from sample mean parameters (black). Both panels use observed radius of maximum wind.

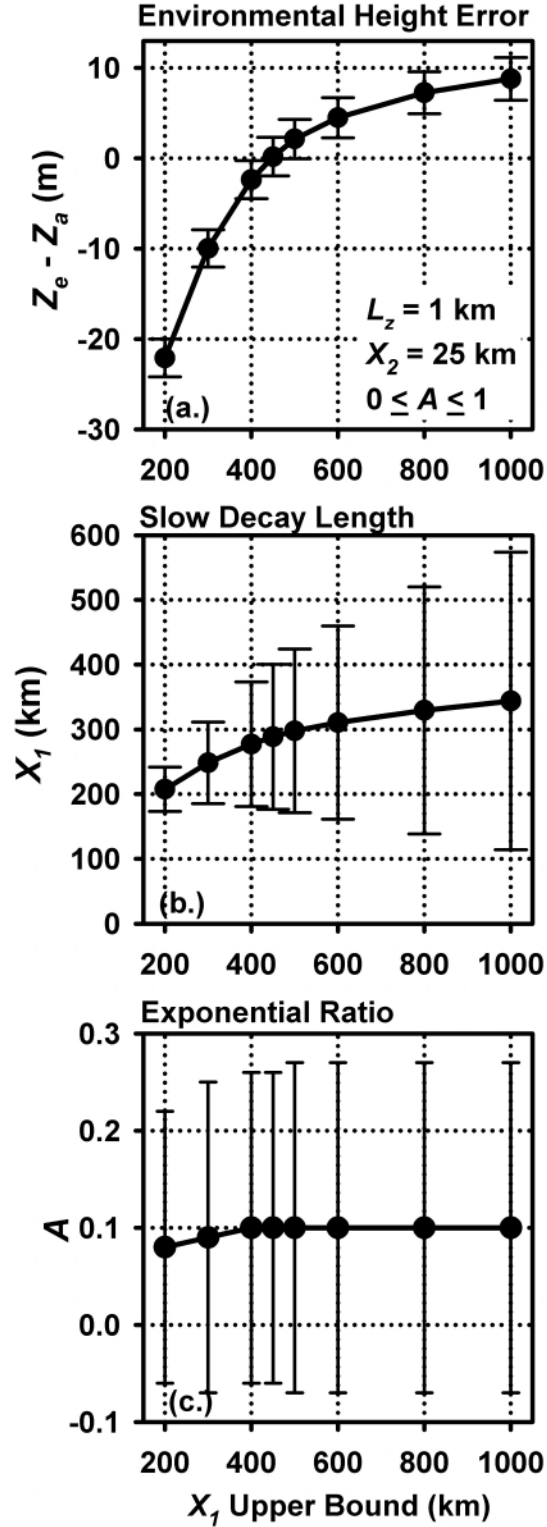


Fig. 8. Variation of (a.) difference between computed and climatological environmental geopotential heights, (b) outer exponential decay length and (c.) fraction of the profile contributed by the shorter exponential with 25 km decay length as functions of the Lagrange-multiplier constraint on the maximum longer decay length for dual-exponential profiles.

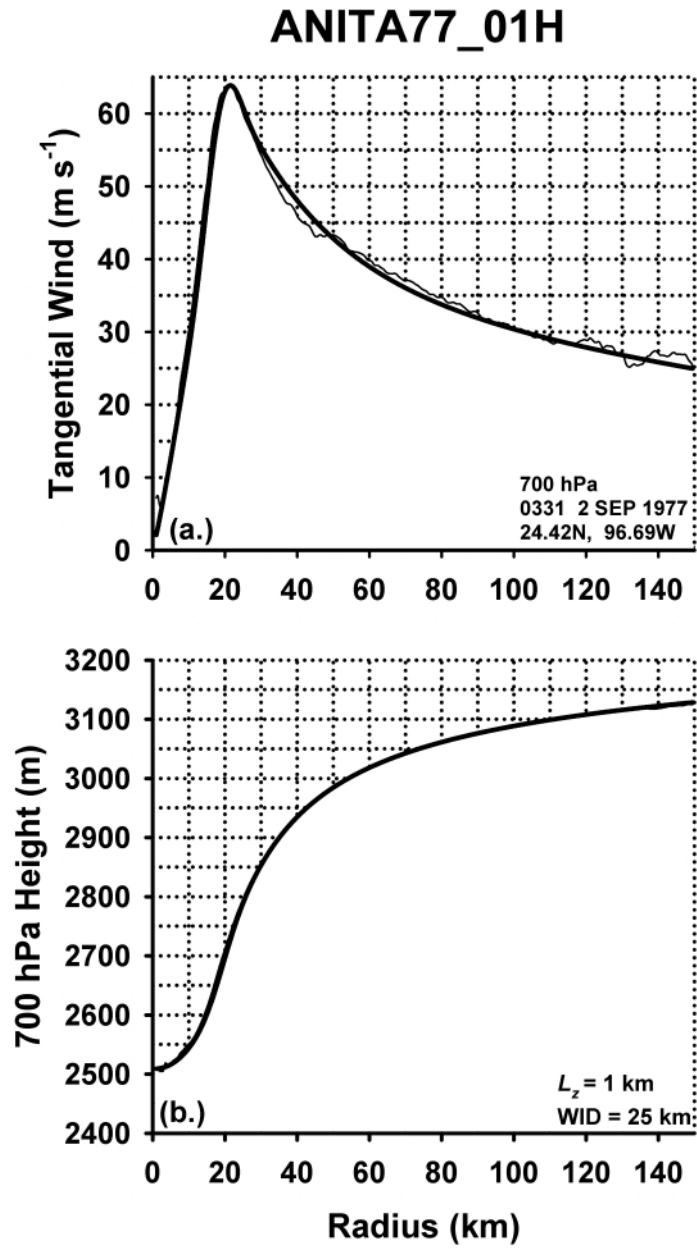


Fig. 9. Dual-exponential (a.) wind and (b.) geopotential height profiles fitted to Hurricane Anita of 1977.

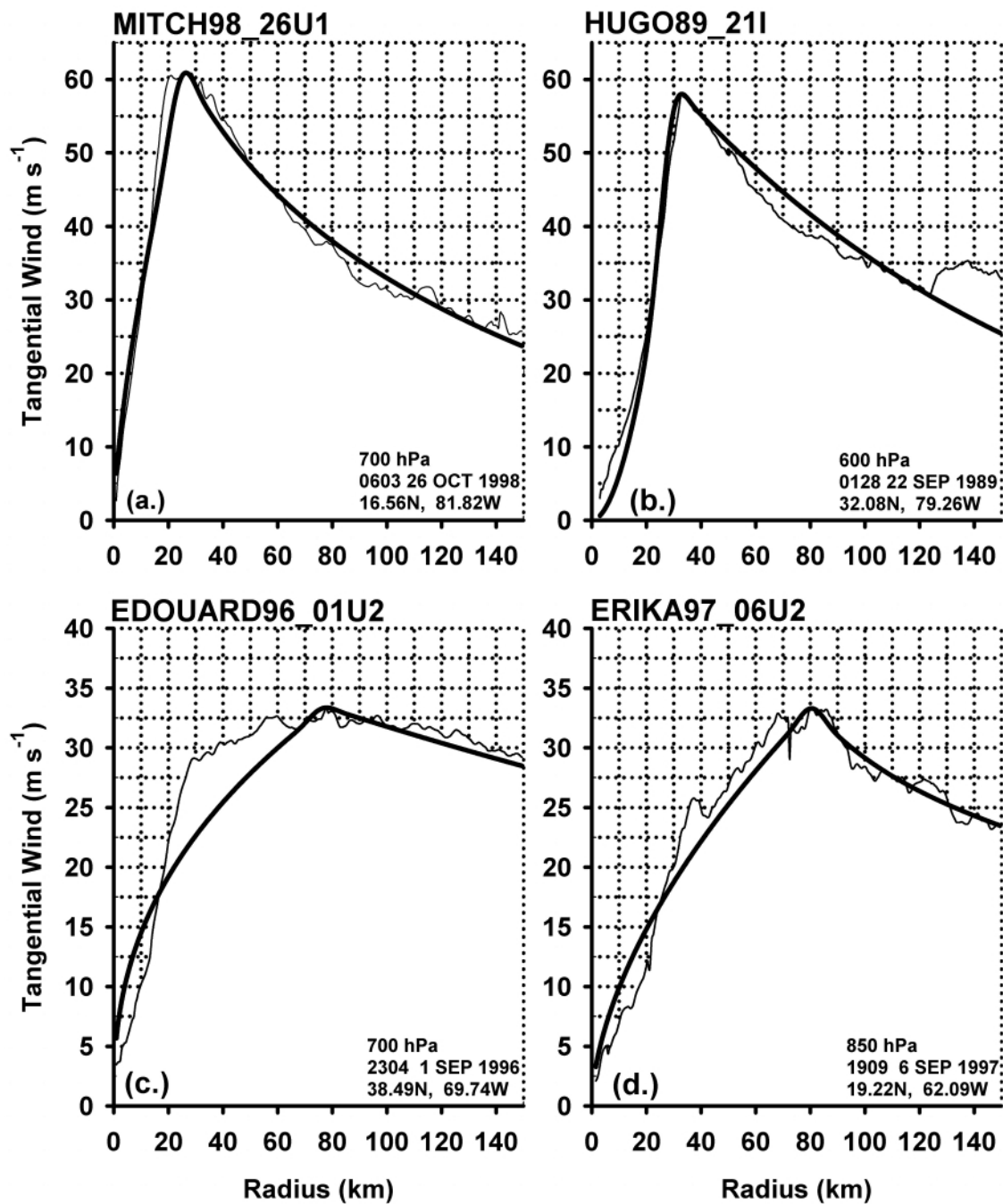


Fig. 10. Dual-exponential wind profiles fitted to Hurricanes (a.) Mitch of 1998, (b.) Hugo of 1989, (c.) Edouard of 1996, and (d.) Erika of 1997.

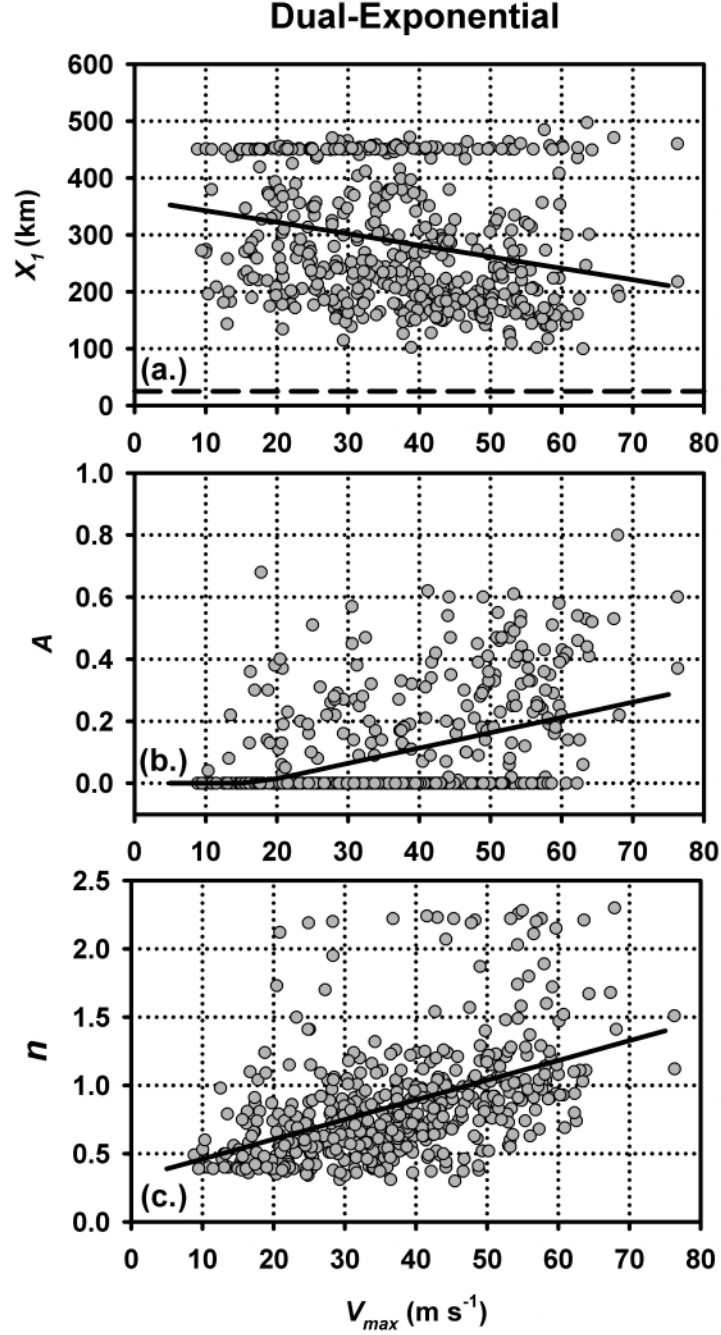


Fig. 11. Scatter plots and regression lines as functions of maximum wind for fitted (a.) dual-exponential longer (solid) and shorter (dashed, fixed at 25 km) decay lengths, (b.) fraction that the shorter decay length contributes to the outer profile, and (c.) inner vortex power-law exponent. Shaded circles represent parameters values determined by the fitting algorithm.

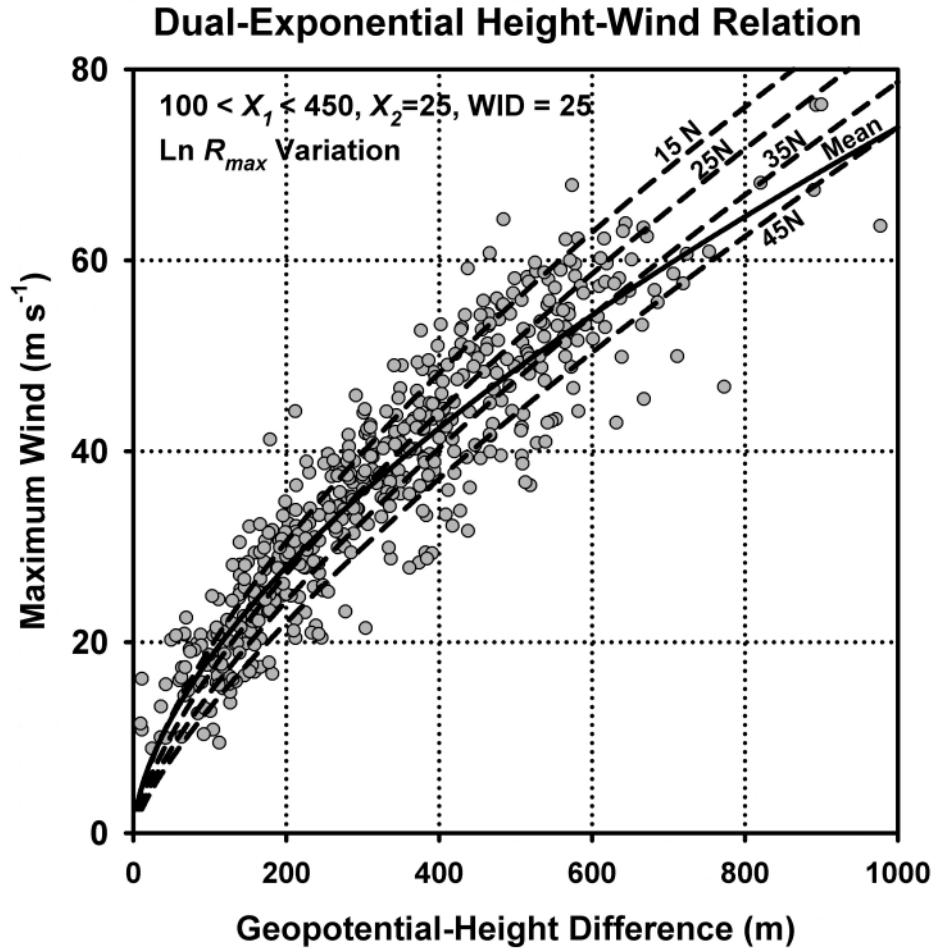


Fig. 12. Height-wind relation computed from the dual-exponential profiles. Shaded circles represent observed wind speed as a function of the difference between climatological environmental geopotential height and observed central geopotential height. Dashed curves are power-law approximations (12.1-12.4) to the height difference computed from the gradient-wind relation using parameters estimated linearly from maximum wind and latitude at 15E, 25E, 35E, and 45E latitude. The solid curve is the height-wind relation (12.5) computed with the sample-mean values of the parameters.

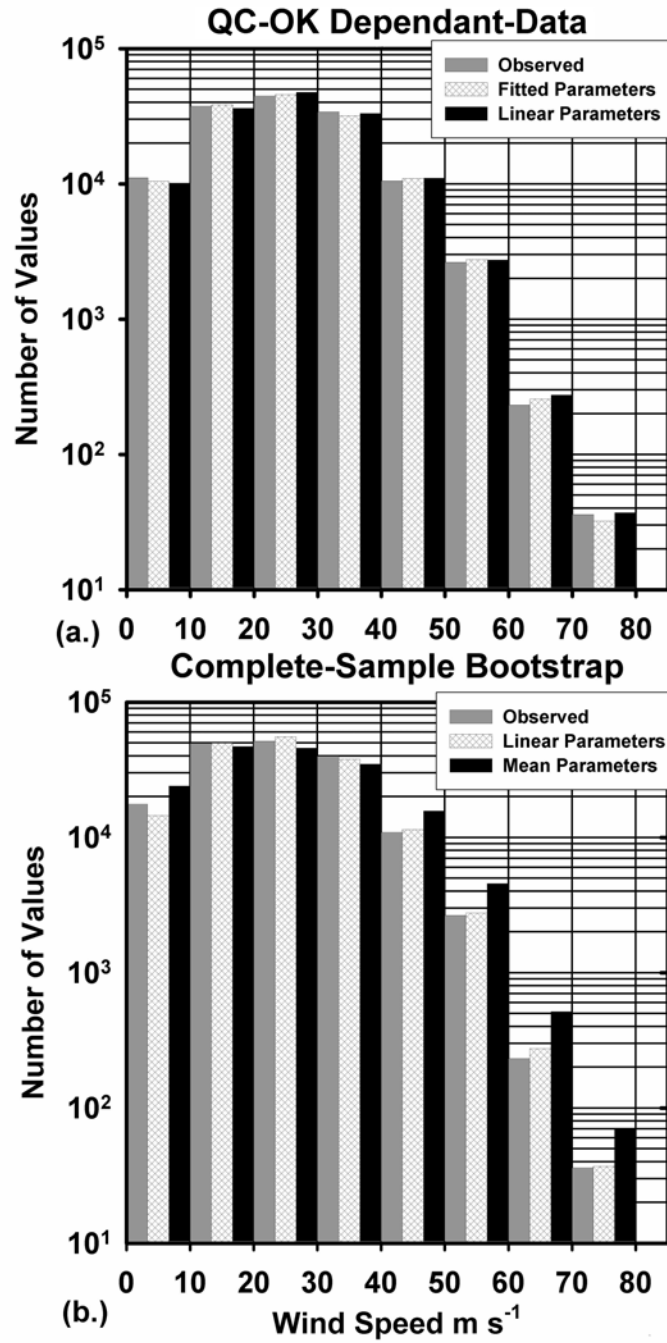


Fig 13

Fig. 13. Histograms of observed and dual-exponential profile with $X_2 = 25$ km wind speeds: (a.) Dependant-data observed (gray), computed from profile-specific fitted parameters (cross-hatched), and computed from linearly estimated parameters for profiles that passed QC (black). (b.) Complete-sample observed (gray), computed from linearly estimated parameters (cross-hatched), and computed from sample mean parameters (black). Both panels use observed radius of maximum wind.

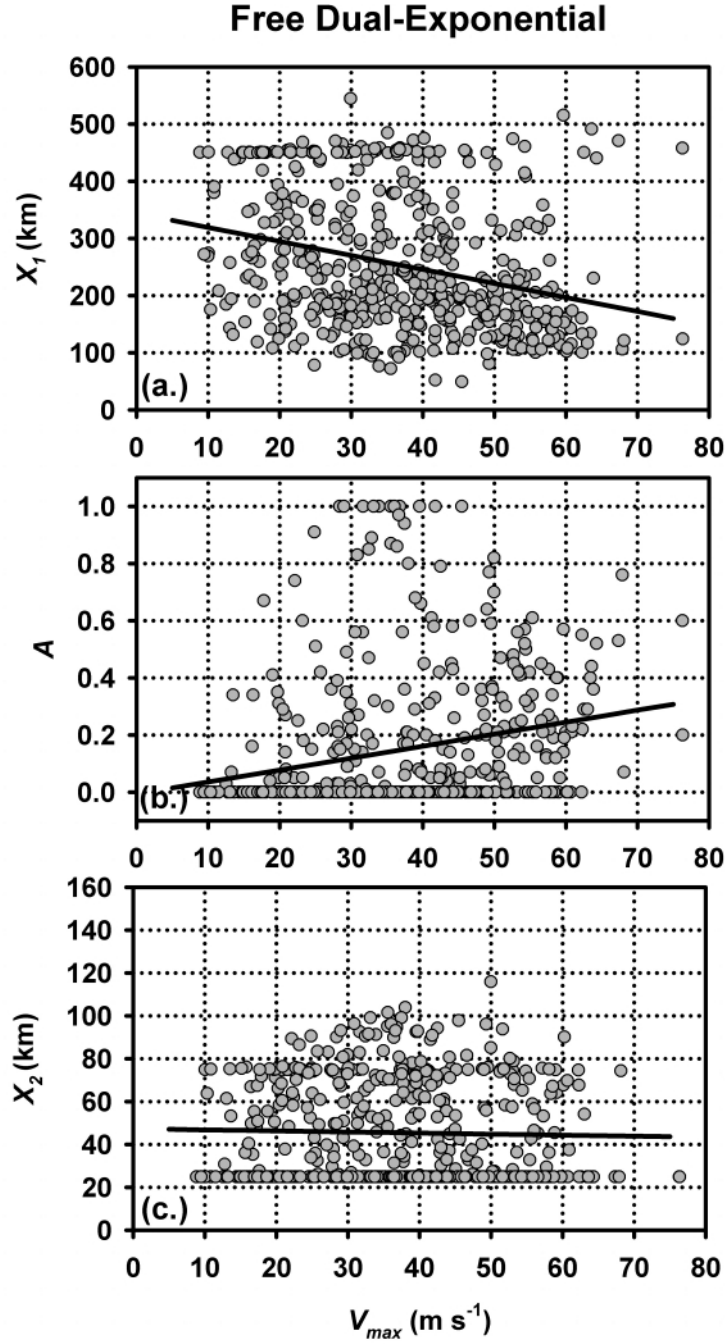


Fig. 14. Scatter plots and regression lines as functions of maximum wind for fitted (a.) free, dual-exponential, longer decay length, (b.) fraction that the shorter decay length contributes to the outer profile and (c.) free, dual-exponential, shorter decay length. Shaded circles represent parameter values determined by the fitting algorithm.

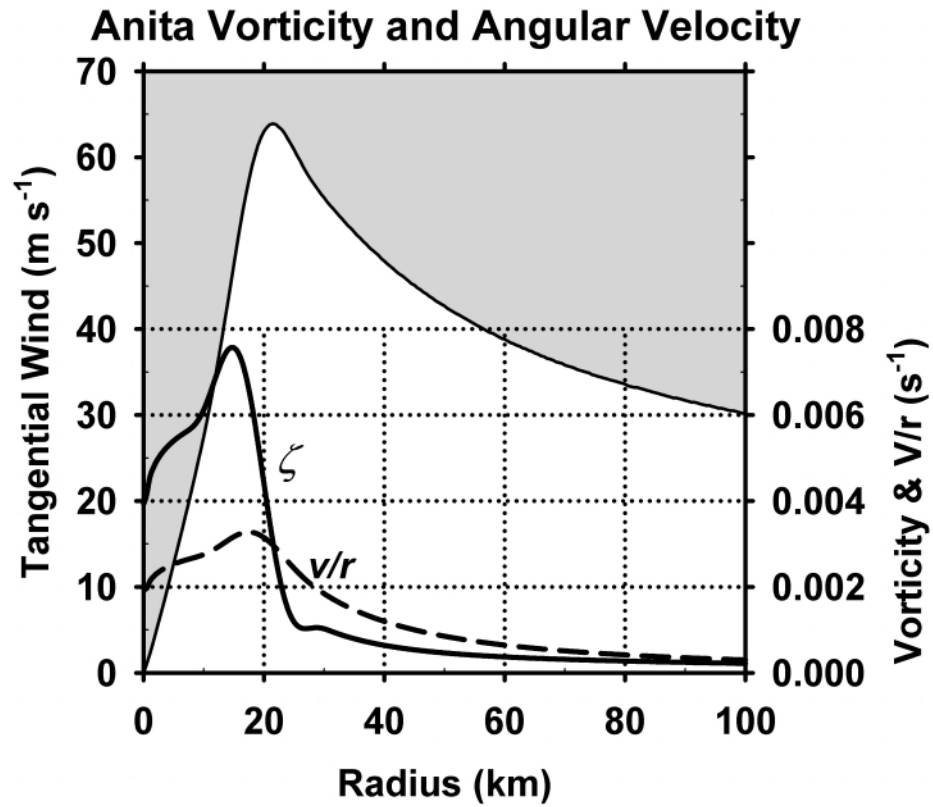


Fig. 15. Vorticity (solid) and angular velocity (dashed) for the dual-exponential profile with $X_2 = 25$ km fitted to Hurricane Anita of 1977, thin line separating white and gray areas.

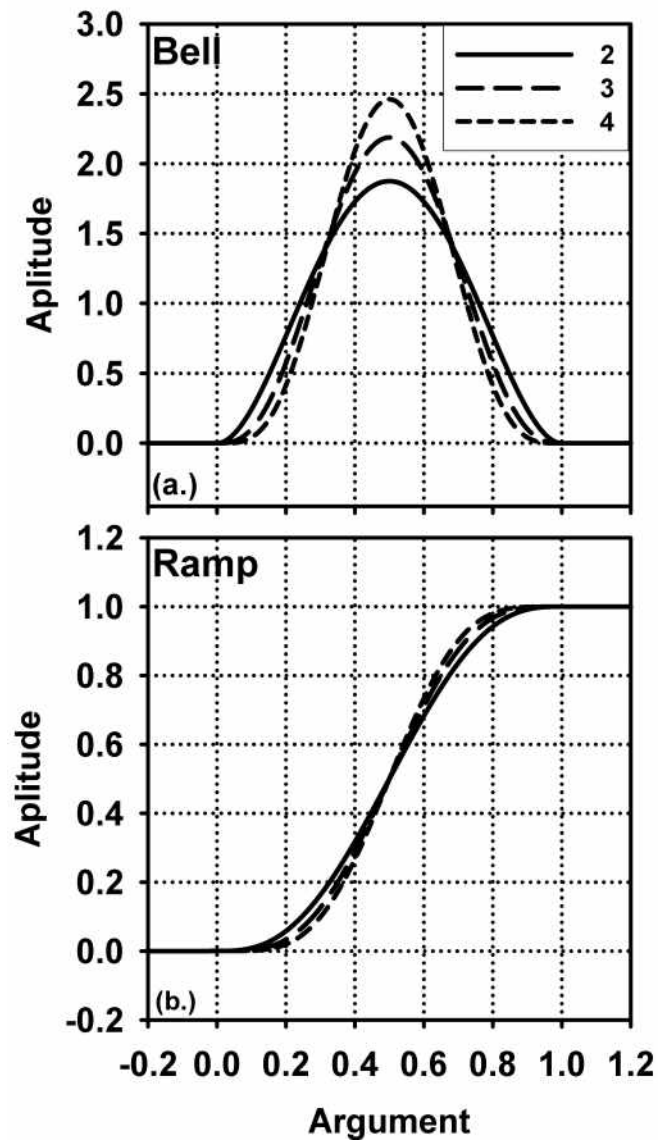


Fig. A1. Polynomial bell and ramp functions computed from (A1) and (A2).